Li et al. Journal of Translational Medicine (2025) 23:279
https://doi.org/10.1186/s12967-025-06280-1

Journal of Translational Medicine

RESEARCH Open Access

Nicotinamide mononucleotide combined with PJ-34 protects microglial cells from lipopolysaccharide-induced mitochondrial impairment through NMNAT3-PARP1 axis

Jia Li[1†], Xiao-Yu Cheng[2†], Rui-Xia Ma[1], Bin Zou[1], Yue Zhang[1], Miao-Miao Wu[1], Yao Yao[3*] and Juan Li[1,4*]

Abstract

Lipopolysaccharide (LPS) is known to induce cell injury and mitochondrial dysfunction, which are pivotal in neuroinflammation and related disorders. Recent studies have demonstrated the potential of nicotinamide mononucleotide (NMN) and poly(ADP-ribose) polymerase-1 (PARP1) inhibitors to enhance mitochondrial function. However, the underlying mechanisms have not been fully elucidated. This study investigates the impact of NMN in conjunction with PJ-34, a PARP1 inhibitor, on LPS-induced mitochondrial damage, focusing on nicotinamide mononucleotide adenylyl transferase 3 (NMNAT3) -PARP1 axis. The results showed that LPS treatment led to down-regulation of NMNAT3 (decreased 58.72% at 1 μM), up-regulation of PARP1 (enhanced 22.78% at 1 μM), thereby impairing mitophagy and mitochondrial function. The negative effects can be mitigated through supplementation with NMN and PJ-34. Specifically, compared to the LPS group, the expression of NMNAT3 increased by 63.29% and PARP1 decreased by 27.94% at a concentration of 400 μM NMN. Additionally, when 400 μM NMN was combined with 5 μM PJ-34, PARP1 expression decreased by 21.99%. Mechanistic studies reveal that NMN and PJ-34 counteracted the detrimental effects by promoting the binding of FoxO1 to the *PINK1* promoter to activate the PINK1/Parkin mediated mitophagy pathway. Further experimental results demonstrate that the down-regulation of NMNAT3 can activate PARP1 and inhibit the initiation of autophagic processes. Consequently, targeting the NMNAT3-PARP1 signaling pathway holds promise for the development of novel therapeutic strategies to alleviate mitochondrial damage-related disorders.

Keywords Neuroinflammation, NMN, NMNAT3, PARP1, Mitochondrial function, C57BL/6J mice, LPS

†Jia Li and Xiao-Yu Cheng contributed equally to this article.

*Correspondence:
Yao Yao
20070007@nxmu.edu.cn
Juan Li
20070018@nxmu.edu.cn
[1]School of Pharmacy, Ningxia Medical University, Yinchuan 750004, People's Republic of China
[2]Department of Neurology and Clinical Research Center of Neurological Disease, The Second Affiliated Hospital of Soochow University, Suzhou 215004, People's Republic of China
[3]School of Basic Medical Sciences, Ningxia Medical University, Yinchuan 750004, People's Republic of China
[4]Key Laboratory of Ningxia Ethnomedicine Modernization, Ningxia Engineering and Technology Research Center for Modernization of Characteristic Chinese Medicine, Ministry of Education, Ningxia Medical University, Yinchuan 750004, People's Republic of China

Introduction

Neuroinflammation is a cardinal feature in the pathogenesis of various neurological conditions and plays a critical role in brain injury surveillance and response [1, 2]. Recent studies show that the pathological process of neuroinflammation is accompanied by mitochondrial dysfunction [3]. Neuroinflammation and mitochondrial dysfunction are involved in the primary pathophysiology of almost all neurodegenerative diseases [4, 5].

Nicotinamide adenine dinucleotide (NAD^+) is a critical intracellular messenger molecule with dual functions of signal transduction and cell metabolism [6]. A decline in the concentration of NAD^+, especially mitochondrial NAD^+, is observed during aging, resulting in mitochondrial dysfunction and the decrease of ATP production [7]. Nicotinamide mononucleotide (NMN) is a direct precursor of NAD^+ [8]. Recent studies confirm that NMN can attenuate cell activation, thereby suppressing inflammation responses [9, 10]. NMN adenylyl transferase 3 (NMNAT3), a specific enzyme for mitochondrial NAD^+ synthesis, shows great potential as a key target for mitochondrial diseases [11, 12]. Emerging evidence suggests that NMN enhances the expression of NMNAT3 in intestinal stem cells of aged mice, thereby delaying gut aging [13]. However, further research is still needed to understand the impact of NMN on NMNAT3 in glial cells and to elucidate the subsequent mechanisms.

Poly(ADP-ribose) polymerase-1 (PARP1) is a crucial NAD consuming enzyme located in the nucleus [14]. It metabolizes nuclear NAD^+ to produce nicotinamide (NAM) and poly (ADP-ribose) (PAR) polymers [15]. PARP1 is regulated by its cofactor NAD^+ and inhibited by the reaction product NAM [16]. The levels of PAR polymer indicate PARP1 enzymatic activity [17]. The PAR polymer has been recognized as a novel signal for cell death, capable of triggering the release of apoptosis-inducing factors (AIFs) from mitochondria, which subsequently leads to cell death. This form of cell death, known as parthanatos, is primarily induced by the overactivation of PARP1 [18]. Furthermore, the hyperactivation of PARP1 depletes NAD^+, leading to ATP loss and the initiation of mitochondrion-dependent necroptosis [19]. PARP1 inhibitors can improve mitochondrial health [20, 21]. Additionally, PARP1 plays an essential role in maintaining genomic integrity, DNA repair, and regulating activity of transcription factor such as p53, NF-κB, and FoxOs [22, 23].

NMN exhibits the dual roles of acting as an inhibitor of PARP1 and serving as a supplement for NAD^+, and thus presents itself as a promising candidate for neuroprotection [24]. Numerous studies have reported a protective effect of NMN on mitochondria, with possible mechanisms involving enhance mitochondrial biogenesis and mitophagy [25, 26]. However, NMN can elevate the levels of PAR polymer [18], which induce depolarization of mitochondrial membrane potential (MMP) and mitochondrial dysfunction [27]. Our study revealed that NMN exacerbated the depolarization damage of MMP in lipopolysaccharide (LPS)-induced BV2 cells for the first time. This adverse effect can be mitigated by the concurrent administration of a PARP1 inhibitor.

The combined effects of NMN and PARP1 inhibitor PJ-34 in regulating mitochondrial function has not been reported, and the mechanism is unclear. Therefore, this study aimed to investigate the therapeutic effects of NMN and PJ-34, and further explore the potential mechanisms involving NMNAT3 and PARP1 in neuroinflammatory protection. Our results confirmed the downregulation of NMNAT3, the upregulation and activation of PARP1, and mitochondrial function damage in LPS induced neuroinflammation. These effects can be reversed by supplementing with NMN and PARP1 inhibitor PJ-34. The study highlights a novel pathological manifestation of NMNAT3 deficiency in neuroinflammation. It reveals the critical role of the NMNAT3-PARP1 axis and elucidates a new therapeutic strategy using NMN combined with PARP1 inhibitors in neuroinflammation.

Materials and methods

Animals

Male C57BL/6J mice (6–8 weeks, 18–22 g) were purchased from the Experimental Animal Center of Ningxia Medical University. All animal experiments were conducted strictly in accordance with the Provision and General Recommendation of Chinses Experiments Animals Administration Legislation and approved by the Ethic Committee of Ningxia Medical University (Approval No. IACUC–NYLAC-2022-N180). The mice were raised in cages with freely available food and water under constant environmental temperature and humidity (22 ± 1 °C and 45-55%, respectively). Mice were adapted to the environment for 1 week prior to experimentation.

Animal experiment procedure

Twenty-four mice were randomly divided into two groups with twelve in each group, namely the control group and LPS group. After anesthetization with 50 mg/kg ketamine and 5 mg/kg xylazine, control group mice were intracerebroventricular (*i.c.v.*) -injected with normal saline (4 μL per mouse), and LPS group mice were subjected to an *i.c.v.* injection of LPS (L8880, Solarbio, China) (5 μg/μL, 4 μL per mouse). Dosages of LPS used to induce neuroinflammation in mice range from 10 ng to over 20 μg [28–30]. Dose of 20 μg LPS per mouse was used to induce inflammation, without severe systemic responses, and no mice died in the experiments. Mice were sacrificed 7 days after injection. Three mice in each

group were used for immunofluorescence and three for western blotting.

Histologic immunofluorescent staining

The brain tissues were fixed in 4% paraformaldehyde, then transferred to 70% ethanol, and dehydrated through a serial alcohol gradient. Tissues were embedded in a paraffin wax block and cut into 4 μm thin sections ($n = 5$; Servicebio, China). All sections were dewaxed in xylene, rehydrated through decreasing concentrations of ethanol, and washed in distilled water. After antigen retrieval in sodium citrate, sections were incubated with 3% hydrogen peroxide for 15 min to block endogenous peroxidase activity. The sections were then blocked with 10% serum for 1 h and incubated with primary antibodies NMNAT3 (1:100, sc-390443, Santa Cruz, CA, USA) or PARP1 (1:200, DF7198, Affinity, OH, USA) at 4℃ overnight. Then sections were washed three times with PBST before being incubated with biotinylates secondary antibodies anti-rabbit (1:50,000, A21020, Abbkine, China) or anti-mouse IgG (1:50,000, A21010, Abbkine, China) for 1 h at room temperature. DAPI (C0065, Solarbio, China) was added at last for nuclear staining. The sections were digitized with Revolve Gen2 high resolution fluorescence microscope (Echo, USA) and Pannoramic 250 Flash scanner (3DHISTECH, Hungary). Three images were obtained from each section. The quantitative statistics were analyzed by Fiji software (Image J version 1.54 m, National Institutes of Health, MD, USA).

Western blot analysis

Tissue or cells were washed in an ice-cold PBS and lysed with Lysis Buffer (P0013, Beyontime, China) containing protease inhibitors, phosphatase inhibitors and PMSF (100 mM). The protein concentration was determined by using a BCA protein quantitative detection kit (G2026-200T, Servicebio, China). Equal amounts of total protein lysates were loaded on SDS-PAGE gels and electrophoresed at 80 V for 30 min and 120 V for 90 min. Protein was transferred to polyvinylidene fluoride (PVDF) membranes at 300 mA for 60 min. Membranes were blocked with 5% non-fat dry milk in TBST for 2 h at room temperature. Membranes were incubated at 4℃ overnight with different primary antibodies: NMNAT3 (1:200, sc-390443, Santa Cruz, CA, USA), PARP1 (1:1,000, DF7198, Affinity, OH, USA), PAR polymer (1:1,000, 4335-MC-100, Trevigen, MD, USA), Beclin1 (1:200, sc-48341, Santa Cruz, CA, USA), p-ULK1 (1:1,000, AF4387, Affinity, OH, USA), ULK1 (1:200, sc-390904, Santa Cruz, CA, USA), LC3 (1:200, sc-398822, Santa Cruz, CA, USA), p62 (1:200, sc-48402, Santa Cruz, CA, USA), Tomm20 (1:1,000, AF5206, Affinity, OH, USA), PINK1 (1:200, sc-518052, Santa Cruz, CA, USA), Parkin (1:200, sc-32282, Santa Cruz, CA, USA), p-Drp1 (Ser616) (1:1,000, AF8470, Affinity, OH, USA), Drp1 (1:1,000, Abcam, ab184247, MA, USA), Mfn2 (1:200, sc-515647, Santa Cruz, CA, USA), Opa1 (1:200, sc-393296, Santa Cruz, CA, USA), p-TBK1(Ser172) (1:1,000, AF8190, Affinity, OH, USA), TBK1 (1:200, sc-52957, Santa Cruz, CA, USA), OPTN (1:200, sc-166576, Santa Cruz, CA, USA), β-actin (1:3,000, AF7018, Affinity, OH, USA), GAPDH (1:1,000, AF7021, Affinity, OH, USA) and Tubulin-β (1:1,000, AF7011, Affinity, OH, USA). The following day, membranes were incubated with anti-rabbit (1:50,000, A21020, Abbkine, China) or anti-mouse IgG (1:50,000, A21010, Abbkine, China) second antibodies for 1 h at room temperature. Blots were incubated with Enhanced ECL Luminescent Liquid (IN0004, Invigentech, CA, USA). Luminescence was detected by gel imaging system (Amersham Imager 600, General Electric Company, NJ, USA). The relative intensity of bands was quantified using Image J software (version 1.54 m, National Institutes of Health, MD, USA).

Cell culture and treatment

BV2 cells were obtained from the Shanghai Institute of Life Science Cell Resource Center. The cells were cultured in DMEM medium with 10% (v/v) fetal bovine serum and 1% penicillin/streptomycin. Microglial activation model was induced by 1 μg/mL LPS [31, 32] (M9524, Abmole, TX, USA) which was followed by different concentration of NMN (S31451, Shanghai Yuanye Bio-Technology, China) or PJ-34 (HY-13688 A, MCE, NJ, USA) treatment.

Enzyme-linked immunosorbent assay (ELISA)

Concentrations of cytokines in cells, including TNF-α and IL-6 were measured by Sandwich ELISA kits (H052-1-2 and H007-1-2, Nanjing Jiancheng Bioengineering Institute, China) following the manufacturer's instructions. Absorbance at 450 nm was measured using a microplate reader (Thermo Scientific, MA, USA).

Cell viability assay

BV2 cells were plated in 96-well plates (5×10^3 cells/well) and treated with different concentrations of LPS, NMN or PJ-34. The cells were incubated with 3- (4,5-dimethylthiazol-2-yl) -2,5-diphenyltetrazolium bromide (MTT) at a final concentration of 1 mg/mL for 4 h. The MTT solution was removed, and 100 μL of DMSO was added to dissolve the MTT formation. After incubating for 10 min at 37 °C, the absorbance was measured at 570 nm on microplate reader (TECAN, Switzerland). The optical density of the formazan formed in control cells was considered to represent 100% viability.

MMP determination

The MMP (MMP, ΔΨm) of BV2 cells was measured using a JC-1 (C2005, Beyontime, China) according to

the manufacturer's instructions. Cells were seeded in 6-well plates (4×10^5 cells/well). MMP was measured 16 h after dosing. Cells were harvested and washed with PBS and incubated with JC-1 at 37℃ for 30 min. After that, fluorescence was detected by BD FACSCelesta™ flow cytometer (BD Biosciences, CA, USA), and the data were incubated with the FlowJo™ Software v10 (BD Life Sciences, OR, USA). MMP was estimated by measuring the fluorescence of free JC-1 monomers (green) and JC-1 aggregates in mitochondria (red) and the results were expressed as the percentage of control based on the ratio of JC-1 aggregates to monomers.

Determination of ATP content

ATP generation in the BV2 cells was measured using an Enhanced ATP Assay Kit (S0027, Beyontime, China) according to the manufacturer's instructions. Cells were seeded in 6-well plates (4×10^5 cells/well). ATP levels were measured 24 h after dosing. The concentration of ATP was calculated according to an ATP strandard curve and reported as nmol/mg of protein.

Plasmid transfection

The BV2 cells were divided into two groups according to the transfection conditions: shCtrl and shNMNAT3. All plasmids were sequenced and confirmed for sequence accuracy. The shRNA vectors and the corresponding control shRNA vector were obtained from Fenghuibio (FengHui Biological Technology, China). The sequences were as follows: shNMNAT3#1, 5'-ATGACCCGGAAA GGTACATCT-3'; shNMNAT3#2, 5'-CAGCACTGCC AGAGTTGAAC-3'; shNMANT3#3, 5'-ATATGCACC TGCGCTTGTTTG-3'. The cells were transfected using LipoFiter 3.0™ Transfection Reagent (HB-TRLF3-1000, HanBio Technology, China) with serum-free medium in advance. After 6 h, the medium was changed to complete medium. After 48 h, the expression of green fluorescent protein was observed under an inverted fluorescence microscope, and the transfection efficiency was calculated by western blots analysis. After that, drug administration was performed.

Confocal microscopy

For confocal analysis, the cells were fixed with 4% paraformaldehyde for 15 min at room temperature. Membrane was ruptured with Triton X100 (T8200, Solarbio, China) for 10 min. The cells (3×10^5 cells/well) were incubated with 100 nM Mito-Tracker Red CMXRos (C1049B, Beyontime, China) in the dark for 20 min at 37℃. Samples were incubated with primary antibody Parkin (1:150, sc-32282, Santa Cruz, CA, USA) or LAMP1 (1:150, sc-20011, Santa Cruz, CA, USA) overnight at 4℃. The following day, the slides were washed with PBS and incubated with a secondary antibody (1:1000, A21010, Abbkine, China) at room temperature for 1 h. The nucleus was stained using DAPI (C0065, Solarbio, China). The images were acquired via a laser confocal microscope (Zeiss, Germany). Colocalization was estimated using the Colocalization plug-in of Fiji software (Image J version 1.54 m, National Institutes of Health, MD, USA). Overlap between the expression protein was quantified using Pearson's colocalization coefficients.

Transmission electron microscopy(TEM)

The cells were harvested and fixed with fixative for TEM (G1102, Servicebio, China) at 4℃. Next, the cells were fixed with 1% OsO4 in 0.1 mol/L PBS for 2 h at room temperature, folled by dehydration with gradient alcohol. Subsequently, the samples were embedded, and then baked in an oven at 60℃ for 48 h. The samples were sectioned into ultrathin Sect. (60 nm) using an ultramicrotome. The ultrastructure of mitochondria was observed using a transmission electron microscope (HT7700, HITACHI, Japan).

Quantitative real-time polymerase chain reaction (RT-qPCR)

Total RNA was extracted from BV2 cells using RNA simple Total RNA Kit (DP419, TIANGEN, China) and was reverse transcribed according to the manufacturer's protocol (RevertAid First Strand cDNA Synthesis Kit, #K1622, Thermo Scientific, MA, USA). Amplification reactions were performed with a *PerfectStart*™ Green qPCR SuperMix (AQ601, TransGen Biotech, China) and specific primers (Table 1) on a Bio-Rad iQ5 Real-Time PCR detection system (Bio-Rad, CA, USA). Quantification of *PINK1*, *NMNAT3 and PARP1 mRNA* standardized to *GAPDH* mRNA levels was performed using the $2^{-\Delta\Delta Ct}$ method.

Chromatin Immunoprecipitation(ChIP) assay

ChIP assay was conducted using the ChIP assay Kit (P2078, Beyotime, China) according to the manufacturer's instructions. Briefly, cells were cross-linked with 1% formaldehyde for 30 min at room temperature, and the reaction was quenched by 5 min of incubation in glycine.

Table 1 Primers used for RT-qPCR

Genes	Forward	Reverse
Mouse PINK1	CGCCTATGAAATCTTTGGGC	GCACTGCCTTGGCCATAGAA
Mouse NMNAT3	GACATCTGACTGGATTCGGGTG	ACCAAGCCGAACTTCTCCACTA
Mouse PARP1	GCGACGCTTATTACTGTACTGGG	CTTCTTGAGGTAGGATATTTCTCGG

Cell monolayer was harvested in ice-cold PBS containing protease inhibitors. Chromatin fragments was achieved by using Micrococcal Nuclease (MNase, D7201S, Beyotime, China). Fragments DNA of 500–1000 bp was precleared with Protein A + G Agarose/Salmon Sperm DNA and then immunoprecipitated with anti-FoxO1 antibody (sc-374427, Santa Cruz, CA, USA) or normal mouse IgG (A7028, Beyotime, China) for 16 h at 4℃. Immunoprecipitated DNA amplification was performed by using a *PerfectStart*™ Green qPCR SuperMix.

Statistical analyses

All statistical analyses were conducted with the GraphPad Prism version 8.3.0 (GraphPad software, CA, USA). Data were obtained from multiple repeats of different biological experiments to obtain the mean values and standard error of the mean (SEM) displayed throughout. All data were tested for normality applying the Shapiro-Wilk test. After normality confirmation, comparisons between multiple groups were made by one-way ANOVA followed by Tukey or Dunnett post hoc tests. For comparisons between two groups, an unpaired two-tailed Student's *t*-test was conducted. Every possible comparison between the study groups was considered. A value of $p < 0.05$ was considered statistically significant.

Results

LPS down-regulates NMNAT3, up-regulates and activates PARP1, leading to mitochondrial impairment

We conducted western blot analyses to detect NMNAT3 expression in the whole brain and hippocampus of mice after LPS administration. The results demonstrated a significant reduction in NMNAT3 expression in both tissues compared to the control group (Additional file 1: Fig. S1a, b). Additionally, we used immunofluorescence experiments to confirm the decrease in NMNAT3 expression levels in the cortex and hippocampus following LPS exposure (Additional file 1: Fig. S1d, e). Furthermore, our results confirmed a significant increase in PARP1 expression and PARylation modification levels within the same model (Additional file 1: Fig. S1a, c, f, g).

In subsequent cell experiments, it was observed that LPS could down-regulate NMNAT3 in a dose-dependent manner. 1 μg/mL of LPS could increase the levels of inflammatory factors (TNF-α and IL-1β), while a lower concentration, i.e., 0.5 μg/mL, could lead to the down-regulation of NMNAT3 (Fig. 1a-d). These observations suggest that the abnormal expression of NMNAT3 may precede neuroinflammation. In agreement with the results of animal experiments, LPS stimulation considerably down-regulates NMNAT3, as well as up-regulates and activates PARP1 in BV2 cells (Fig. 1e-g). The consistent effects of LPS on NMNAT3 and PARP1 were also observed at the transcriptional level (Fig. 1h, i).

Next, we employed double fluorescence staining of mitochondria using JC-1 and measured MMP through flow cytometry and confocal microscopy. The obtained results exhibited a decrease in MMP following LPS induction (Fig. 2a, b). ATP is recognized as the primary energy source in living organisms [33]. Our study unequivocally identified a substantial reduction in ATP levels induced by LPS, thereby confirming its direct negative impact on mitochondria (Fig. 2c).

To examine the ultrastructure of mitochondria, TEM analysis was performed. Mitochondria in the control group exhibited normal morphology. However, cells treated with LPS showed typical morphological changes indicative of damage, including mitochondrial swelling, membrane rupture, and cristae fragmentation or disappearance. Additionally, the images demonstrated that LPS-induced cells had smaller mitochondrial size compared to the control group (Fig. 2d, e).

Lysosomal-associated membrane protein 1 (LAMP1) is a marker located on the outer membrane of lysosomes, which are primarily found in the cytoplasm [34]. The fusion of lysosomes and mitochondria is the final step in the process of mitophagy; as such, the colocalization of LAMP1 and mitochondria can be used to monitor mitophagy [35]. In immunofluorescence colocalization experiments, LAMP1 was labeled with green fluorescence, mitochondria were labeled with red fluorescence. The yellow pixels indicate areas of colocalization between LAMP1 and mitochondria. Compared with the control group, we observed a reduction in the intensity of yellow pixels after LPS treatment, indicating incomplete mitophagy (Fig. 2f, g).

The down-regulation of NMNAT3 activates PARP1, inhibits the initiation of autophagy, and leading to mitochondrial impairment

In this part, we used shNMNAT3 plasmid to investigate its impact on PARP1 activity (the levels of PARylation modification) and autophagy initiation process (the levels of p-ULK1 and Beclin1), as well as the mitochondrial function (MMP and ATP).

When autophagy is initiated, mammalian target of rapamycin (mTOR) is dephosphorylated, resulting in the disassociation of mTORC1 from the serine-threonine protein kinase, Unc-51-like kinase 1 (ULK1). Subsequently, the PI3K III complex is recruited to the location of autophagosome formation by the activated ULK1 complex [36]. Therefore, ULK1 acts as an initiator of autophagy, and its activity is regulated by different sites. Phosphorylation at Ser317 and Ser777 activates ULK1, while phosphorylation at Ser757 inhibits its activation [37]. Beclin1 is a subunit of the PI3K complex, plays a crucial role in initiating the formation of autophagosomes by binding to autophagic precursors [38]. Under

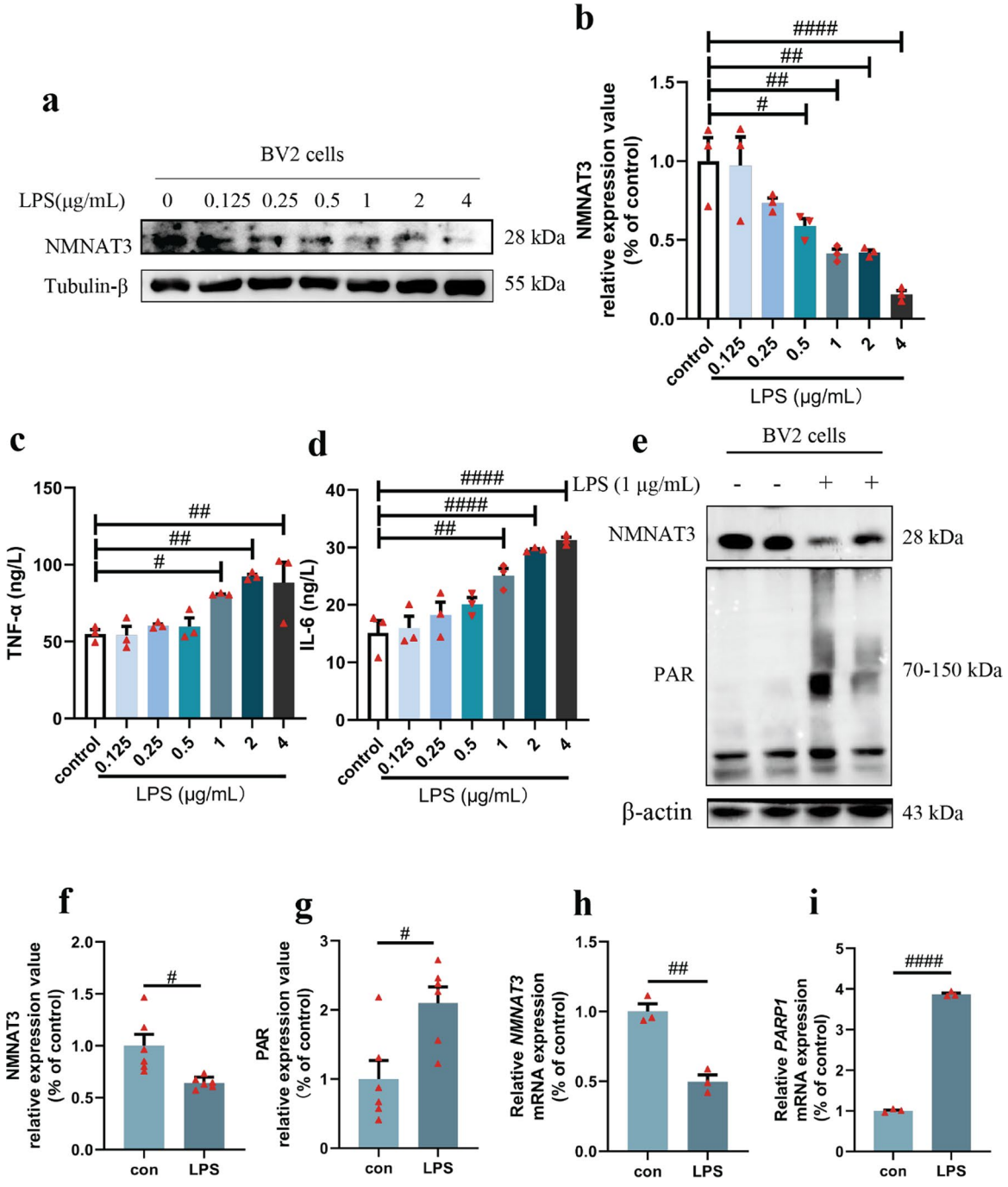

Fig. 1 LPS down-regulates NMNAT3, up-regulates and activates PARP1, and induces inflammatory factor release in BV2 cells. **(a)** Representative immunoblots of NMNAT3 in BV2 cells treated with different concentration of LPS, and control group. Tubulin-β was used as a loading control. **(b)** Quantification of relative expression levels of NMNAT3 protein in each group ($n=3$; $^{\#}$, $p<0.05$; $^{\#\#}$, $p<0.01$; $^{\#\#\#\#}$, $p<0.0001$). **(c)** Quantification of TNF-α in BV2 cells treated with different concentration of LPS ($n=3$; $^{\#}$, $p<0.05$; $^{\#\#}$, $p<0.01$). **(d)** Quantification of IL-6 in BV2 cells treated with different concentration of LPS ($n=3$; $^{\#\#}$, $p<0.01$; $^{\#\#\#\#}$, $p<0.0001$). **(e)** Representative immunoblots of NMNAT3 and PAR polymer in BV2 cells with or without LPS (±LPS) treatment. β-actin was used as a loading control. **(f)** Quantification of relative expression levels of NMNAT3 protein in each group ($n=6$; $^{\#}$, $p<0.05$). **(g)** Quantification of total PARylation levels in each group ($n=6$; $^{\#}$, $p<0.05$). **(h)** Quantification of *NMNAT3* mRNA expression of BV2 cells were detected by RT-qPCR ($n=3$; $^{\#\#}$, $p<0.01$). **(i)** Quantification of *PARP1* mRNA expression of BV2 cells were detected by RT-qPCR ($n=3$; $^{\#\#\#\#}$, $p<0.0001$). Data are presented as mean ± SEM. Statistical analyses were performed with One-way ANOVA followed by Dunnett's post hoc test (**b**, **c**, **d**) or unpaired Student's t-test (**f**, **g**, **h**, **i**). Abbreviations: LPS, lipopolysaccharide; NMNAT3, Nicotinamide mononucleotide adenylyl transferase 3; PAR, poly ADP-ribose; PARP1, Poly (ADP-ribose) polymerase-1

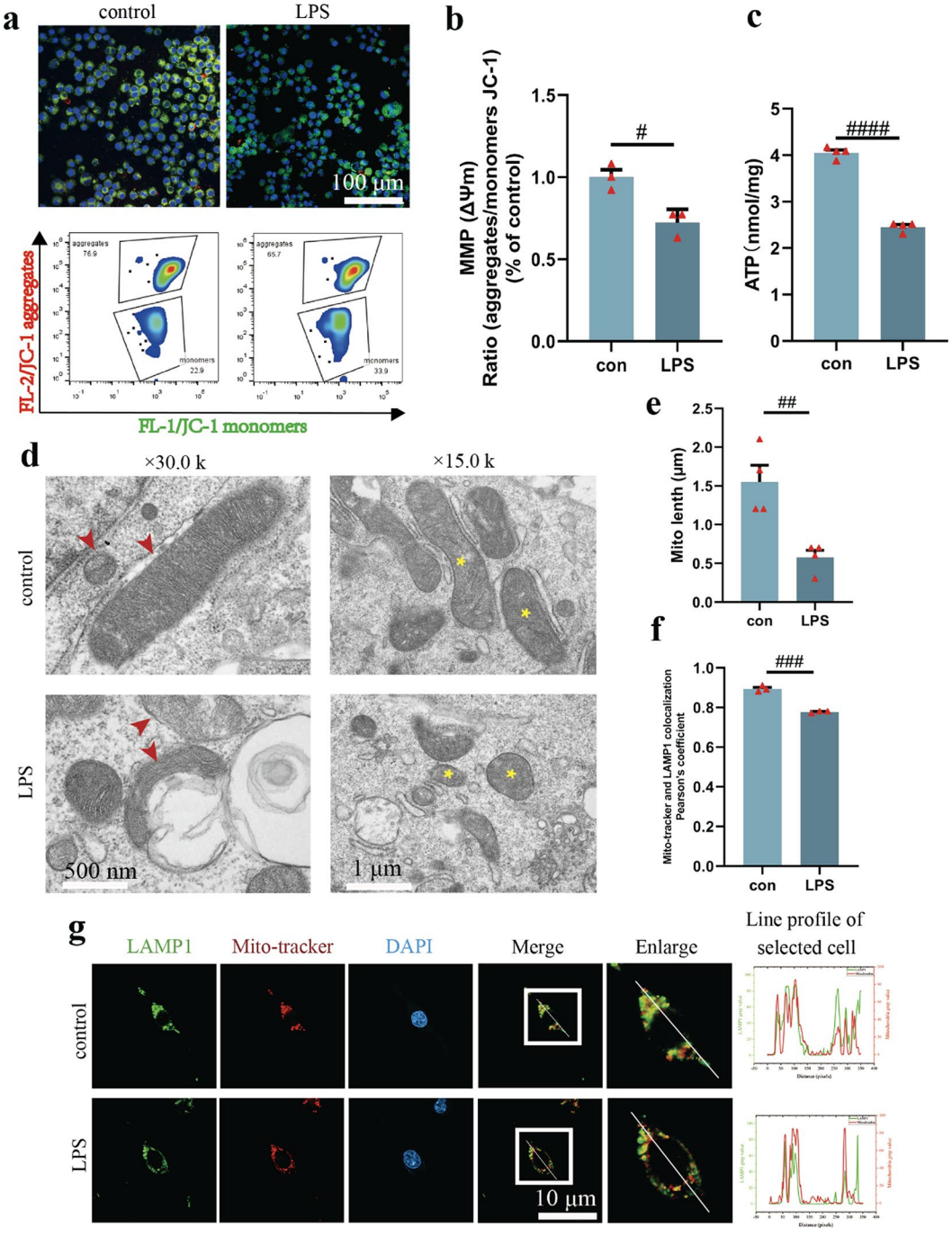

Fig. 2 LPS causes impaired mitochondrial function, morphology and mitophagy in BV2 cells. **a.** Representative images of JC-1 staining in BV2 cells analyzed by flow cytometry and confocal microscope with or without LPS (± LPS) treatment. The cells were incubated with JC-1 for 30 min before visualized by confocal microscope and flow cytometry detection. Scale bar, 100 μm. **b.** Quantification of the MMP in BV2 cells with or without LPS (± LPS) treatment ($n = 3$; $^{\#}$, $p < 0.05$). **c.** Quantification of ATP levels in BV2 cells with or without LPS (± LPS) treatment ($n = 4$; $^{\#\#\#\#}$, $p < 0.0001$). **d.** Representative TEM images of BV2 cells with or without LPS (± LPS) treatment. Scale bar: left, 500 nm; right, 1 μm. **e.** Quantitation analysis of mitochondrial length in BV2 cells ($n = 4$; $^{\#\#}$, $p < 0.01$). **f**. Pearson's r value of the colocalization of LAMP1 and mitochondria in BV2 cells ($n = 3$; $^{\#\#\#}$, $p < 0.001$). **g.** Representative images of colocalization of LAMP1 (green) and mito-tracker (red) in BV2 cells with or without LPS (± LPS) treatment. Scale bar = 10 μm. Data are presented as mean ± SEM. Statistical analyses were performed with unpaired Student's t-test (**b**, **c**, **e**, **f**). Abbreviations: LPS, lipopolysaccharide; MMP, Mitochondrial membrane potential; LAMP1, Lysosomal-associated membrane protein 1

normal physiological conditions, a basal level of autophagy is essential for maintaining cellular homeostasis. Insufficient autophagy can result in the buildup of damaged cellular components [38].

Initially, western blot analysis showed a notably down-regulation of NMNAT3 in shNMNAT3 group compared to the shCtrl group (Fig. 3a, b). Subsequently, the findings demonstrated that NMNAT3 down-regulation led to an increase in PARylation level and p-ULK1 (Ser757) expression (Fig. 3a, c, d), a decrease in Beclin1 expression (Fig. 3a, e). Additionally, the results showed that a decrease in ATP levels and MMP in shNMNAT3 group compared to the shCtrl group (Fig. 3f-h). The above results indicate that NMNAT3 knockdown activates PARP1, inhibits the initiation of autophagy, and impairs mitochondrial function.

NMN supplementation up-regulates NMNAT3, down-regulates PARP1, and restores mitophagy

To determine the optimal concentration of NMN that does not compromise cell viability, we conducted an MTT assay. The results demonstrated that NMN at 800 μM significantly decreased cell viability, while 400 μM NMN improved cell viability that had been inhibited by LPS. Based on these findings, we selected NMN doses of 100, 200, and 400 μM for cell administration (Fig. 4a, b). Adding exogenous NMN to the BV2 cell medium mitigated the decrease of NMNAT3 expression and the increase of PARP1 expression induced by LPS (Fig. 4c, d, e). Nevertheless, PARylation modification levels was also increased (Fig. 4c, f).

As shown in Fig. 4g, NAM is both a feedback inhibitor of PARP1 and the precursor of NMN [23, 39]. NMN also contains a nicotinamide pharmacophore that shows potential to inhibit PARP1, but it also increases nuclear NAD^+ formation, leading to higher levels of PARylation modification.

Previous studies have demonstrated that the reduction of NAD^+ [40, 41] and the activation of PARP1 [42, 43] lead to defects in mitophagy. To examine the changes in mitophagy levels, we assessed the expression levels of mitophagy-related proteins. After LPS stimulation, the expression of Beclin1 and the ratio of LC3II/LC3I was significantly decreased, while p62 expression was increased, indicating a blockage in the process of autophagosome degradation (Additional file 1: Fig. S2a-d). As mitophagy involves the degradation of mitochondrial proteins, the elevated Tom20 (a mitochondrial marker) in the LPS group indicates increased mitochondrial content, suggesting a possible barrier to mitophagy (Additional file 1: Fig. S2a, e) [44]. Conversely, treatment with NMN demonstrated an increase in the LC3II/LC3I ratio and Beclin1 expression, as well as a decrease in p62 and Tom20 expression, thereby confirming the ability of NMN to restore impaired mitophagy (Additional file 1: Fig. S2a-e).

Mitophagy is a process that selectively degrades damaged mitochondria, with the PINK1/Parkin-dependent pathway being of particular importance [45]. Depolarization of mitochondria is an established driving force for mitophagy. Depolarized damaged mitochondria lead to the accumulation of PINK1 on the mitochondrial outer membrane. PINK1 further facilitates the recruitment of Parkin to initiate mitophagy [46]. Moreover, PINK1/Parkin-mediated mitophagy requires ubiquitin-binding autophagy receptors such as optineurin (OPTN). Tank-binding kinase 1 (TBK1) is a Ser/Thr kinase that is important for the selective autophagic removal of damaged mitochondria. TBK1 promotes Parkin-mediated mitophagy by phosphorylating NDP52 and OPTN to increase their affinity for ubiquitin, and that OPTN recruits TBK1 onto damaged mitochondria [47].

In this study, the expression of PINK1 and Parkin was significantly decreased, while the p-TBK1/TBK1 and OPTN increased in LPS-induced BV2 cells, which is consistent with previous report [48]. LPS induces inflammatory responses and increases the phosphorylation level of TBK1, and it has been reported that the transcription level of OPTN is elevated after LPS treatment [49]. These results suggest that LPS induced mitophagy damage is mediated through the expression of PINK1 and Parkin but not the TBK1 and OPTN pathway, while supplementation with NMN rescued the expression of these proteins (Fig. S2a, f, g; Fig. S5a-c). To assess the colocalization of Parkin and mitochondrial, we utilized Mitotracker to label mitochondria and visualized Dylight 488-labeled Parkin. We quantified the colocalization between mitochondria and Parkin through Image J software. Under normal conditions, green Parkin colocalizes with red mitochondria, resulting in the formation of yellow dots. The results demonstrated that LPS reduced the number of yellow dots, indicating that the colocalization of Parkin and mitochondria was decreased, and NMN promoted this process (Additional file 1: Fig. S3a, b).

Next, we investigated the effects of NMN on colocalization of LAMP1 and mitochondria. Compared with LPS group, the yellow pixels increased after NMN treatment, indicating mitophagy was enhanced (Additional file 1: Fig. S4a, b).

NMN supplementation increases ATP levels in a dose-dependent manner, but exacerbates MMP depolarization

The results demonstrate that NMN supplementation could effectively elevate ATP content in a dose-dependent manner (Additional file 1: Fig. S4c). Surprisingly, the addition of NMN resulted in a significant decrease in MMP (Additional file 1: Fig. S4d, e). This effect may be

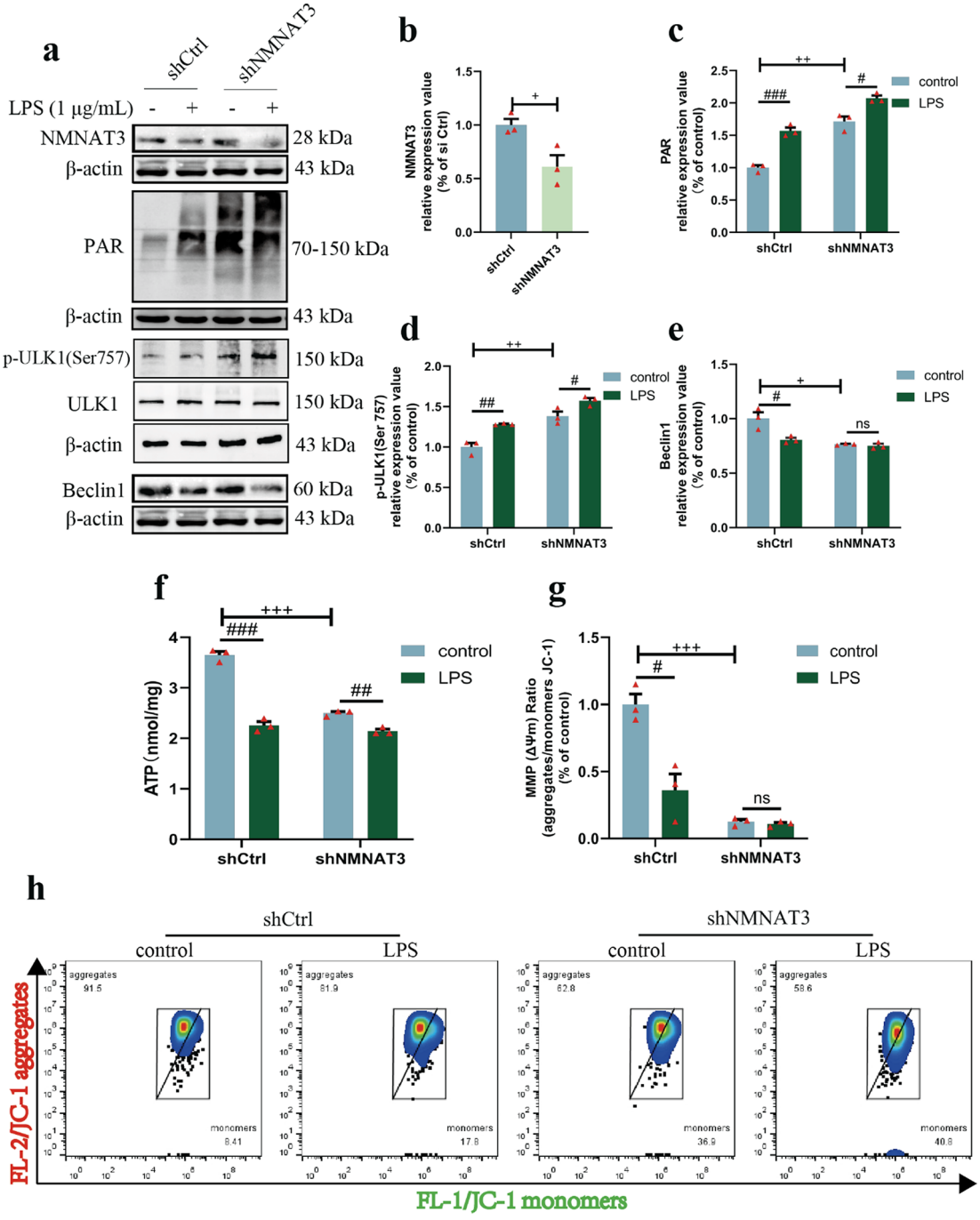

Fig. 3 The down-regulation of NMNAT3 activates PARP1, inhibits the initiation of autophagy, and leading to mitochondrial impairment. **(a)** Representative immunoblots of NMNAT3, PAR polymer, p-ULK1 and Beclin1 in BV2 cells transfected with shRNA. β-actin was used as a loading control. **(b)** Quantitative analysis of NMNAT3 knockdown efficiency ($n=3$; $^{+}$, $p<0.05$). **(c)** Quantification of total PARylation levels in BV2 cells transfected with shRNA ($n=3$; $^{\#}$, $p<0.05$; $^{\#\#\#}$, $p<0.001$; $^{++}$, $p<0.01$). **(d)** Quantification of relative expression levels of p-ULK1 protein in BV2 cells transfected with shRNA ($n=3$; $^{\#}$, $p<0.05$; $^{\#\#}$, $p<0.01$, $^{++}$, $p<0.01$). **(e)** Quantification of relative expression levels of Beclin1 protein in BV2 cells transfected with shRNA ($n=3$; $^{\#}$, $p<0.05$; $^{+}$, $p<0.05$). **(f)** Quantification of ATP levels in BV2 cells transfected with shRNA ($n=3$; $^{\#\#}p<0.01$; $^{\#\#\#}p<0.001$, $^{***}p<0.001$). **(g)** The quantification of the MMP in BV2 cells transfected with shRNA ($n=3$; $^{\#}p<0.05$; $^{+++}$, $p<0.001$) **(h)** Representative images of JC-1 staining in in BV2 cells transfected with shRNA analyzed by flow cytometry. Data are presented as mean ± SEM. Statistical analyses were performed with unpaired Student's t-test (**b**) and multiple t-tests (**c-g**). Abbreviations: LPS, lipopolysaccharide; NMNAT3, Nicotinamide mononucleotide adenylyl transferase 3; PAR, poly ADP-ribose; MMP, Mitochondrial membrane potential; ULK1, Unc-51-like kinase 1

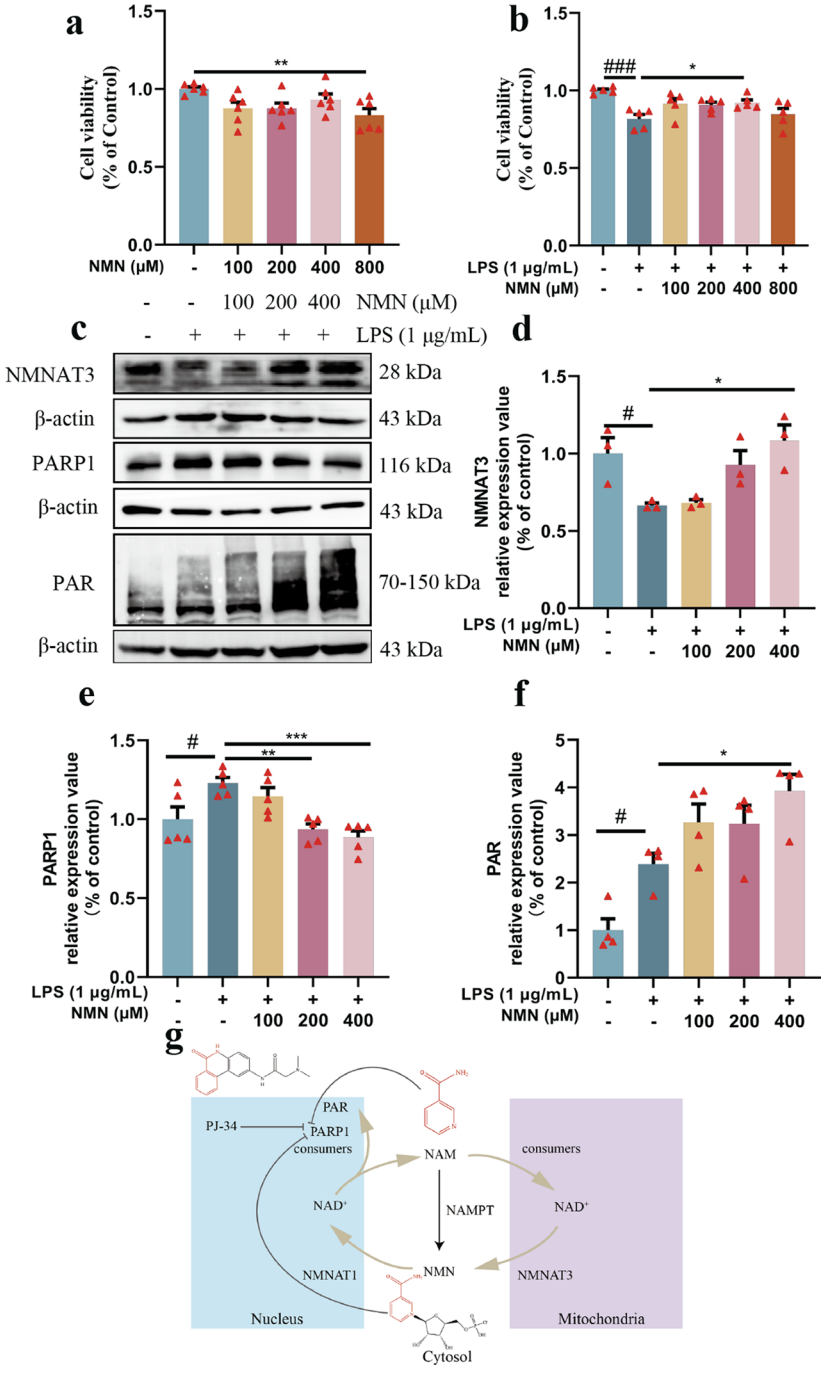

Fig. 4 NMN supplementation up-regulates NMNAT3, down-regulates PARP1 and restores cell viability. **(a)** BV2 cells were treated with different concentrations of NMN for 24 h and viability was measured with MTT assay ($n=6$; **, $p<0.01$). **(b)** BV2 cells were treated with LPS and different concentrations of NMN for 24 h and viability was measured with MTT assay ($n=5$; $^{\#\#\#}$, $p<0.001$; *, $p<0.05$). **(c)** Representative immunoblots of NMNAT3, PARP1 and PAR polymer in LPS-induced BV2 cells treated with different concentration of NMN. β-actin was used as a loading control. **(d)** Quantification of relative expression levels of NMNAT3 protein in each group ($n=3$; $^{\#}$, $p<0.05$; *, $p<0.05$). **(e)** Quantification of relative expression levels of PARP1 protein in each group ($n=5$; $^{\#}$, $p<0.05$; **, $p<0.01$; ***, $p<0.001$). **(f)** Quantification of total PARylation levels in each group ($n=4$; $^{\#}$, $p<0.05$, *, $p<0.05$). **(g)** Schematic representation of production and metabolism of NAD^+ in the nucleus and mitochondria. Abbreviations: NMN, nicotinamide mononucleotide; NMNAT1, Nicotinamide mononucleotide adenylyl transferase 1; NMNAT3, Nicotinamide mononucleotide adenylyl transferase 3; NAD^+, Nicotinamide adenine dinucleotide; NAM, nicotinamide; NAMPT, Nicotinamide phosphoribosyltransferase; PJ-34, 2-(dimethylamino)-N-(5,6-dihydro-6-oxophenanthridin-2yl) acetamide; PARP1, Poly (ADP-ribose) polymerase-1; PAR, poly ADP-ribose. Data are presented as mean ± SEM. Statistical analyses were performed with One-way ANOVA followed by Dunnett's post hoc test (**a**, **b**, **d**, **e**, **f**)

due to a notable increase in PARylation modification levels caused by NMN supplementation.

Evidence suggests that the excessive accumulation of PAR polymer can negatively impact mitochondrial function by triggering the release of AIFs from the mitochondria [50, 51]. The accumulation of PAR polymer within the cytoplasm may directly or indirectly affect mitochondria, thereby disrupting MMP [27, 52]. These provide a possible explanation for the observed decline in MMP following NMN treatment.

NMN supplementation combined with a PARP1 inhibitor jointly restrains PARP1 activity, improves mitochondrial quality

To counteract the increase in the levels of PARylation modification induced by NMN, we added the PARP1 inhibitor, PJ-34. The MTT assay showed that PJ-34 concentrations above 10 μM resulted in a notable decrease in BV2 cell viability (Fig. 5a). Therefore, we selected 5 μM PJ-34 for subsequent experiments. Additionally, the results demonstrated that the simultaneous use of NMN and PJ-34 further enhanced cell viability (Fig. 5b).

Compared with the LPS group, the presence of NMN and PJ-34 markedly suppressed PARP1 expression and activity (Fig. 5c-e). Furthermore, the combined treatment of PJ-34 and NMN resulted in higher ATP content and improved MMP levels (Fig. 5f-h).

The expression of mitophagy-related proteins, when exposed to LPS and NMN, was consistent with the above findings. Following the combined treatment of NMN and PJ-34, there was an increase in Beclin1 expression, an elevation in the LC3-II/LC3I ratio, and a decrease in p62 expression, indicating an enhancement in autophagy flux after inhibiting PARP1 (Fig. 6a-d). Additionally, the expression of PINK1 and Parkin increased (Fig. 6a, e, f), the expression of p-TBK1/TBK1 and OPTN decreased after NMN and PJ-34 treatment (Fig. S5a-c), suggesting an augmented mitophagy process. Immunofluorescence colocalization experiments confirmed that the combination of NMN and PJ-34 led to a significant increase in the colocalization of LAMP1 and mitochondria compared to the LPS group, confirming increased mitophagy (Fig. 6g, h).

As previously mentioned, the TEM results showed that the mitochondria ultrastructure was severely disrupted and the number of smaller mitochondria increased in response to LPS (Fig. 2d, e). We speculate that this damage is associated with impaired mitochondrial dynamics. P-Drp1 (Ser616) translocates to the outer mitochondrial membrane and induces mitochondrial fission, which is a pivotal protein involved in mitochondrial network fragmentation [53], whereas Mfn2 and Opa1 are key proteins for mitochondrial fusion [54]. Our findings demonstrated up-regulation of p-Drp1(Ser616) expression and down-regulation of Opa1 and Mfn2 expression in the LPS-induced BV2 cells, indicating impaired mitochondrial dynamics. Following treatment with NMN and PJ-34, there was a decrease in p-Drp1(Ser616) expression and an increase in Opa1 and Mfn2 expression (Fig. 7a-d). These results, in conjunction with the TEM analysis (Fig. 7e, f), confirmed the recovery of mitochondrial morphology and dynamics.

Overall, these findings support the notion that supplementing NMN along with PJ-34 can effectively restore mitophagy, improve mitochondrial quality, and enhance cell viability.

PARP1 Inhibition enhances PINK1/Parkin-mediated mitophagy by increasing the binding of FoxO1 to the PINK1 promoter

Forkhead box O1 (FoxO1) is a transcription factor involved in various biological processes [55]. Previous studies have established that PARP1 regulates FoxO1, as inhibition of PARP1 leads to an increase in the mRNA levels of *FoxO1* [56]. Additionally, modifications mediated by PARP1 post-translationally may reduce the affinity of FoxO1 for its target genes [56]. Another study confirmed that FoxO1 is involved in the regulation of *PINK1*, which is a key target gene of mitophagy [57].

To investigate whether PARP1 regulates the PINK1/Parkin pathway via FoxO1, we conducted RT-qPCR and ChIP assays. The RT-qPCR experiments demonstrated a significant decrease in *PINK1* mRNA levels under the action of LPS. However, the combination of NMN and PJ-34 showed a noteworthy increase in *PINK1* mRNA levels compared to the LPS group, indicating that PARP1 inhibition can affect *PINK1* expression at the transcriptional level (Fig. 8a). The results of the ChIP assay revealed that LPS reduces the binding of FoxO1 to the *PINK1* promoter, but the combination of NMN and PJ-34 significantly enhances this binding (Fig. 8b). These findings confirm that PARP1 inhibition enhances PINK1-mediated mitophagy by promoting the binding of FoxO1 to the *PINK1* promoter.

The regulation of the binding of FoxO1 to the *PINK1* promoter by PARP1 is illustrated in Fig. 8c-e. Under normal conditions, PARP1 promotes the transcription initiation process of PINK1 by controlling the interaction between FoxO1 and the *PINK1* promoter (Fig. 8c). Activation of PARP1 was observed under the action of LPS, which resulted in the inhibition of *PINK1* transcription by disrupting the binding of FoxO1 to the *PINK1* promoter (Fig. 8d). Conversely, supplementation of NMN combined with a PARP1 inhibitor significantly suppressed the activation of PARP1 and facilitated the binding of FoxO1 to the *PINK1* promoter (Fig. 8e).

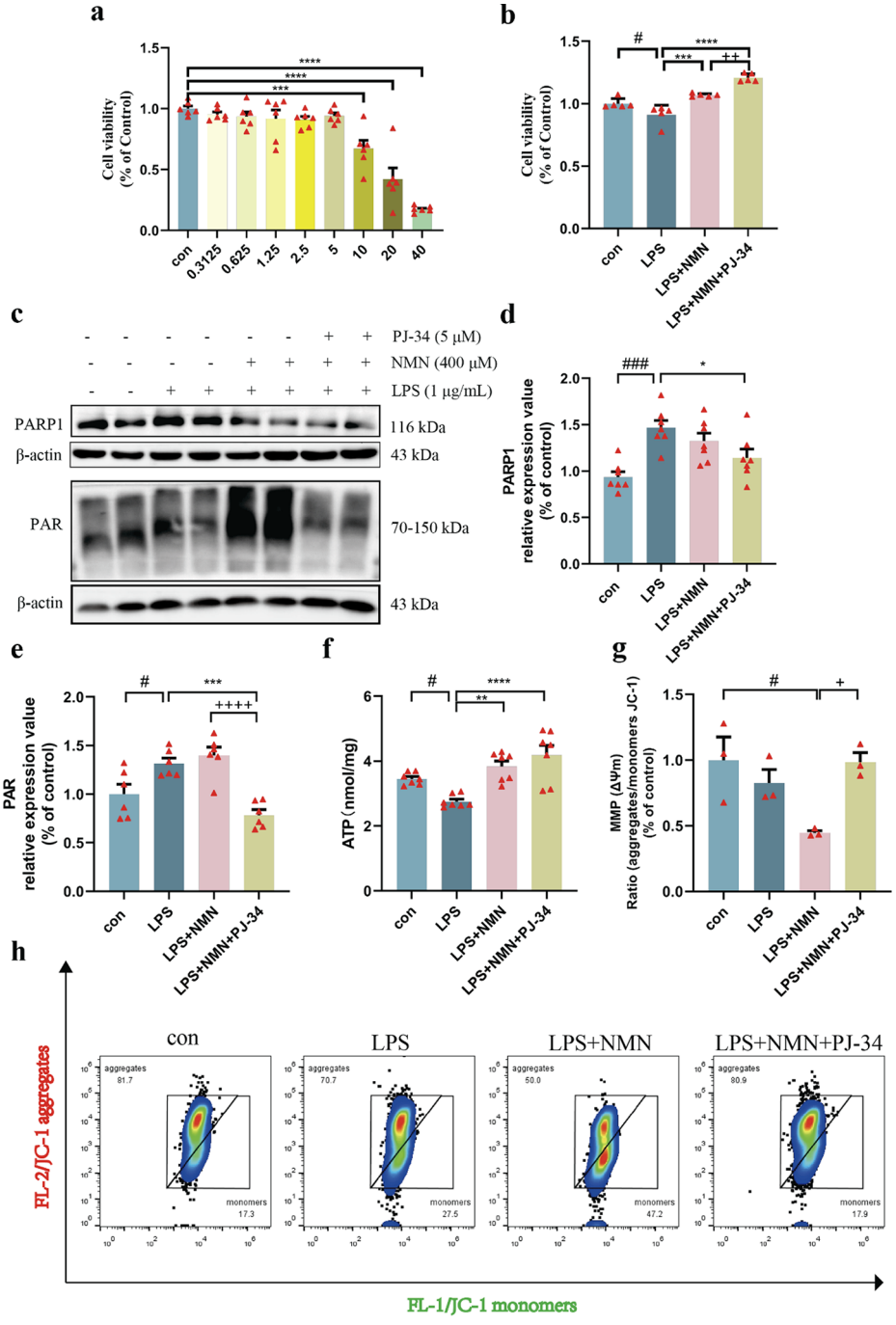

Fig. 5 NMN supplementation combined with a PARP1 inhibitor jointly restrains PARP1 activity, improves mitochondrial quality. **(a)** BV2 cells were treated with different concentrations of PJ-34 for 24 h and viability was measured with MTT assay. ($n=6$; ***, $p<0.001$, ****, $p<0.0001$). **(b)** BV2 cells were treated with NMN and PJ-34 for 24 h and viability was measured with MTT assay ($n=5$; $^{\#}$, $p<0.05$; ***, $p<0.001$; ****, $p<0.0001$; $^{++}$, $p<0.01$). **(c)** Representative immunoblots of PARP1 and PAR polymer in LPS-induced BV2 cells treated with NMN and PJ-34. β-actin was used as a loading control. **(d)** Quantification of relative expression levels of PARP1 protein in each group ($n=6$; $^{\#\#\#}$, $p<0.001$; *, $p<0.05$). **(e)** Quantification of total PARylation levels in each group ($n=6$; $^{\#}$, $p<0.5$; ***, $p<0.001$; $^{++++}$, $p<0.0001$). **(f)** Quantification of ATP levels in LPS-induced BV2 cells ($n=7$; $^{\#}p<0.05$; $^{**}p<0.01$, $^{****}p<0.0001$). **(g)** The quantification of the MMP in LPS-induced BV2 cells ($n=3$; $^{\#}p<0.05$; $^{+}$, $p<0.05$). **(h)** Representative images of JC-1 staining in LPS-induced BV2 cells analyzed by flow cytometry. Data are presented as mean ± SEM. Statistical analyses were performed with One-way ANOVA followed by Dunnett's post hoc test (**a**) or Turkey's post hoc test (**b**, **d**, **e**, **f**, **g**). Abbreviations: LPS, lipopolysaccharide; NMN, nicotinamide mononucleotide; PARP1, Poly (ADP-ribose) polymerase-1; PAR, poly ADP-ribose; MMP, Mitochondrial membrane potential

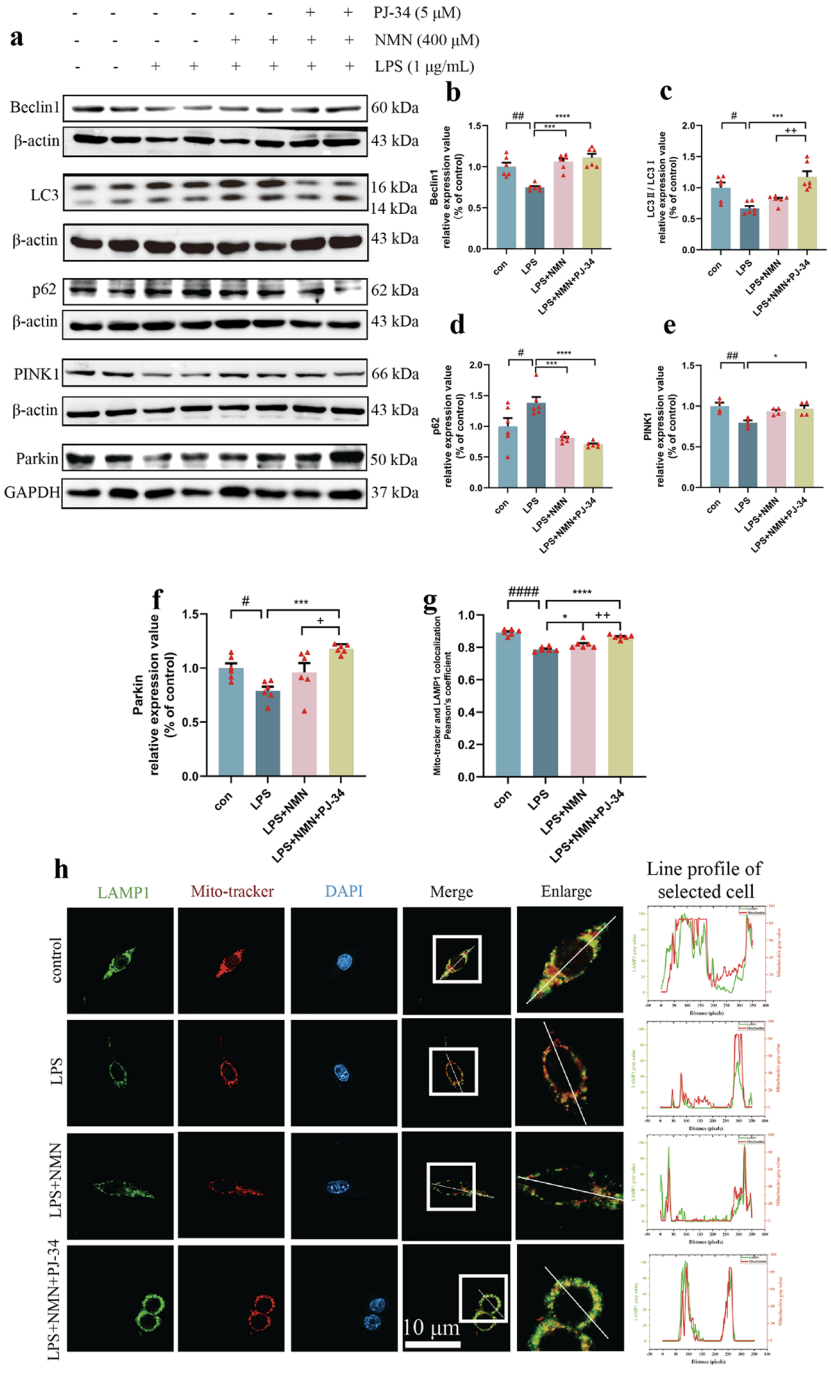

Fig. 6 NMN supplementation combined with a PARP1 inhibitor jointly improves mitophagy. **(a)** Representative immunoblots of mitophagy-related proteins in LPS-induced BV2 cells treated with NMN and PJ-34. GAPDH and β-actin was used as a loading control. **(b)** Quantification of relative expression levels of Beclin1 protein in each group ($n=6$; $^{\#\#}$, $p<0.01$; ***, $p<0.001$; ****, $p<0.0001$). **(c)** Quantification of relative expression levels of LC3II/LC3I in each group ($n=6$; $^{\#}$, $p<0.05$; ***, $p<0.001$; $^{++}$, $p<0.01$). **(d)** Quantification of relative expression levels of p62 protein in each group ($n=6$; $^{\#}$, $p<0.05$; ***, $p<0.001$; ****, $p<0.0001$). **(e)** Quantification of relative expression levels of PINK1 protein in each group ($n=4$; $^{\#\#}$, $p<0.01$; *, $p<0.05$). **(f)** Quantification of relative expression levels of Parkin protein in each group ($n=6$; $^{\#}$, $p<0.05$; ***, $p<0.001$; $^{+}$, $p<0.05$). **(g)** Pearson's r value of the colocalization of LAMP1 and mitochondria in LPS-induced BV2 cells ($n=6$; $^{\#\#\#\#}$, $p<0.0001$; *, $p<0.05$; ****, $p<0.0001$; $^{++}$, $p<0.01$). **(h)** Representative images of colocalization of LAMP1 (green) and mito-tracker (red) in LPS-induced BV2 cells. Scale bar = 10 μm. Data are presented as mean ± SEM. Statistical analyses were performed with One-way ANOVA followed by Turkey's post hoc test (**b-g**). Abbreviations: LPS, lipopolysaccharide; NMN, nicotinamide mononucleotide; PINK1, PTEN induced kinase 1; LAMP1, Lysosomal-associated membrane protein 1

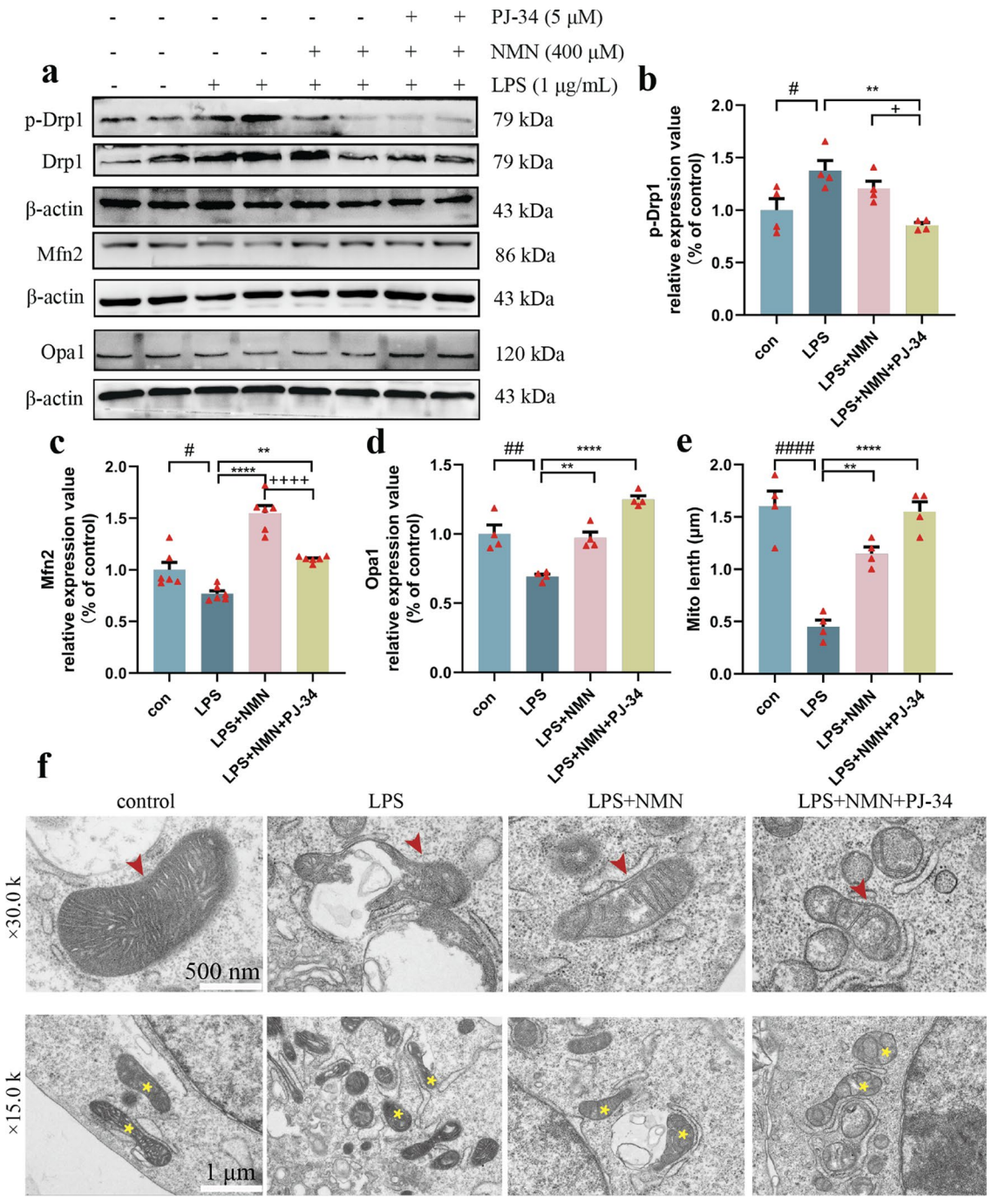

Fig. 7 NMN supplementation combined with a PARP1 inhibitor jointly improves mitochondrial dynamics and mitochondrial morphology. **(a)** Representative immunoblots of mitochondrial fission and fusion proteins in LPS-induced BV2 cells treated with NMN and PJ-34. β-actin was used as a loading control. **(b)** Quantification of relative expression levels of p-Drp1(Ser616) protein in each group ($n=4$; $^{\#}$, $p<0.05$; **, $p<0.01$; $^{+}$, $p<0.05$). **(c)** Quantification of relative expression levels of Mfn2 protein in each group ($n=4$; $^{\#}$, $p<0.05$; **, $p<0.01$; ****, $p<0.0001$; $^{++++}$, $p<0.0001$). **(d)** Quantification of relative expression levels of Opa1 protein in each group ($n=4$; $^{\#\#}$, $p<0.01$; **, $p<0.01$; ****, $p<0.0001$). Data are presented as mean ± SEM. **(e)** Quantitation analysis of mitochondrial length in each group ($n=4$; $^{\#\#\#\#}$, $p<0.0001$; **, $p<0.01$; ****, $p<0.0001$) **(f)** The Representative TEM images of LPS-induced BV2 cells treated with NMN and PJ-34. Scale bar: upper, 500 nm; lower, 1 μm. Data are presented as mean ± SEM. Statistical analyses were performed with One-way ANOVA followed by Turkey's post hoc test (**b-e**). Abbreviations: LPS, lipopolysaccharide; NMN, nicotinamide mononucleotide

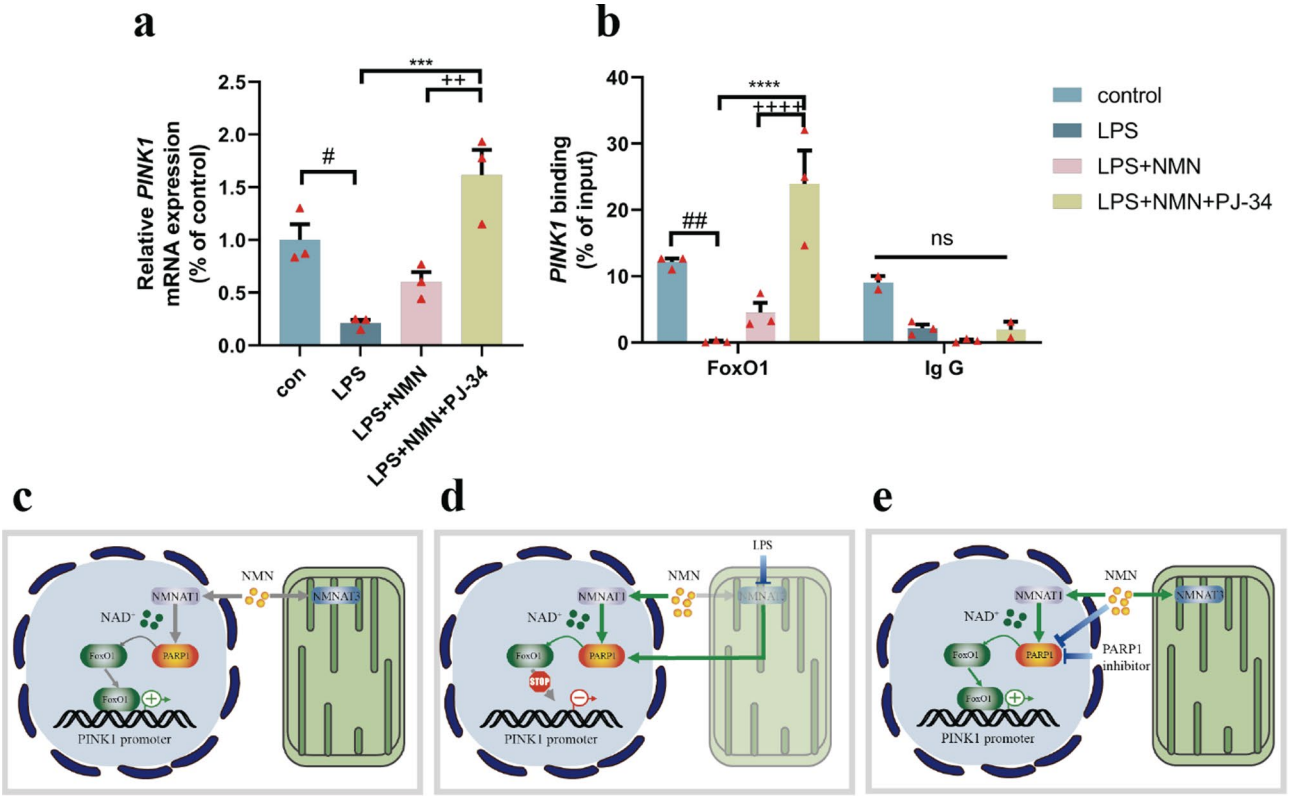

Fig. 8 PARP1 inhibition enhances PINK1/Parkin-mediated mitophagy by increasing the binding of FoxO1 to the *PINK1* promoter. **(a)** The effects of PARP1 on *PINK1* mRNA expression of BV2 cells were detected by RT-qPCR ($n=3$; $^{\#}$, $p<0.05$; ***, $p<0.001$; $^{++}$, $p<0.01$). **(b)** The effects of PARP1 on FoxO1 binding to *PINK1* promoter of BV2 cells were detected by ChIP ($n=3$; $^{\#\#}$, $p<0.01$; ****, $p<0.0001$, $^{++++}$, $p<0.0001$). **(c)** Schematic representation of PARP1 regulates the binding of FoxO1 to *PINK1* promoter. **(d)** Schematic representation of the effect of LPS on the binding of FoxO1 to *PINK1* promoter. **(e)** Schematic representation of the effect of NMN combined with PJ-34 on the binding of FoxO1 to *PINK1* promoter. Abbreviations: LPS, lipopolysaccharide; NMN, nicotinamide mononucleotide; NMNAT1, Nicotinamide mononucleotide adenylyl transferase 1; NMNAT3, Nicotinamide mononucleotide adenylyl transferase 3; NAD^+, Nicotinamide adenine dinucleotide; PARP1, Poly (ADP-ribose) polymerase-1; FoxO1, Forkhead box O1. Data are presented as mean ± SEM. Statistical analyses were performed with One-way ANOVA followed by Turkey's post hoc test (**a**) or Two-way ANOVA followed by Turkey's post hoc test (**b**)

Discussion

In the present study, we observed that NMNAT3 was significantly down-regulated, while PARP1 and its main product, PAR polymer, were significantly up-regulated in LPS induced neuroinflammatory models both in vitro and in vivo. Knockdown of NMANT3 activated PARP1, down-regulated the autophagy initiation process, and leading to mitochondrial impairment. Supplementation of NMN partially rescued the decline in mitochondrial dysfunction. However, we also observed that NMN supplementation led to higher PARylation modification levels and a decrease in MMP. Therefore, we sought to reduce PARylation levels and decrease mitochondrial depolarization injury by using a PARP1 inhibition. Ultimately, we confirmed that supplementation with NMN, in combination with PJ-34, significantly improved mitochondrial quality and cell viability (Fig. 9).

NMNAT3, a mitochondrial NAD^+ synthase, plays a crucial role in maintaining mitochondrial NAD^+ levels [58]. Our data showed significant downregulation of NMNAT3 in the hippocampus and whole brain of C57BL/6J mice in the neuroinflammation model. Subsequently, this down-regulation of NMNAT3 was also found in LPS-induced BV2 cells, potentially occurring prior to the initiation of neuroinflammation. Another study found that LPS-induced acute inflammatory stress damaged NAD^+ synthesis in the liver of aged mice [59]. The liver, containing the largest collection of phagocytic cells in the body, relies on the healthy mitochondrial of these immune cells for proper functioning and normal liver function [60]. Thus, targeting NMNAT3 to regulate macrophage metabolism may help to reduce mitochondrial-related inflammatory injury.

NMN serves as the main intracellular form that regulates NAD^+ levels in compartments and plays a crucial role in interconnecting NAD^+ pools in each subcellular compartment. Recently, Fang et al. confirmed that NMN supplementation can inhibit DOX-induced hepatotoxicity and oxidative stress injury in mice by improving the expression of NMNAT3 [61]. This study also confirmed that supplementation with NMN effectively reversed the down-regulation of NMNAT3, suppressed the expression

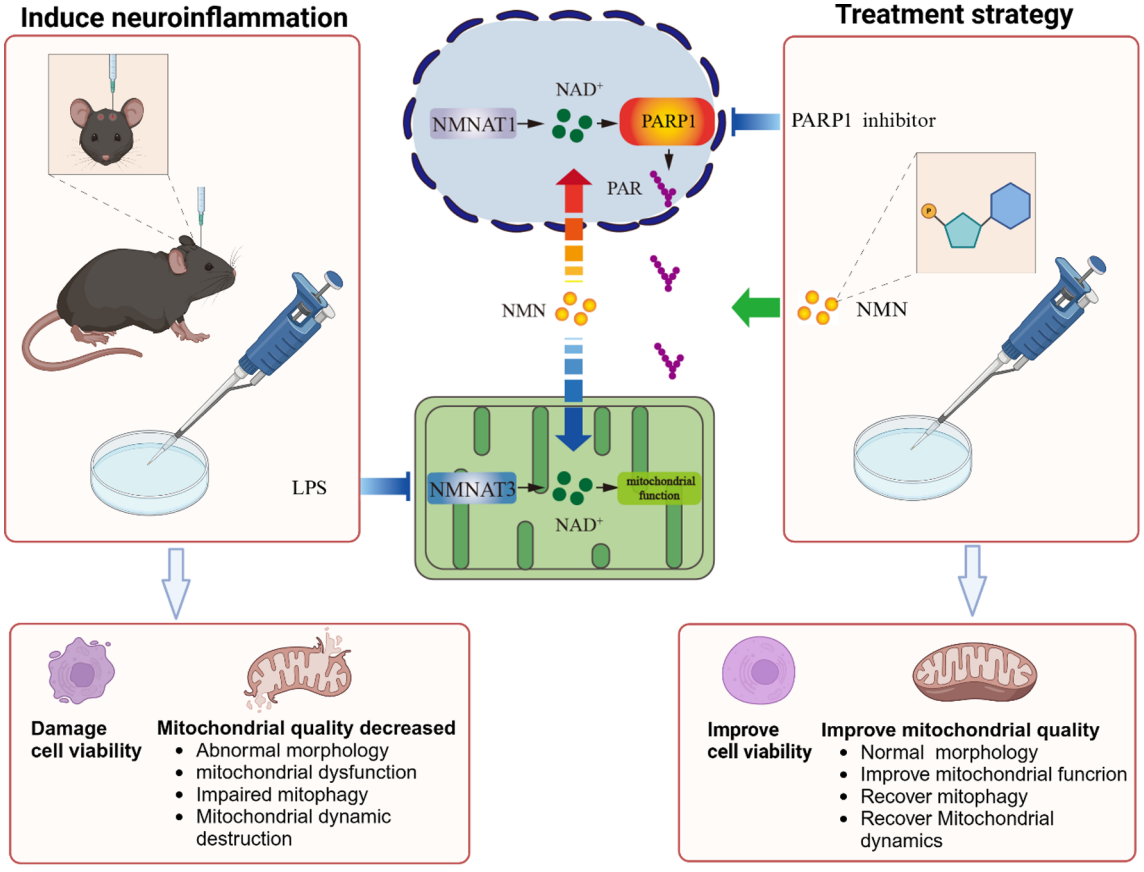

Fig. 9 Schematic depiction of NMN combined with a PARP1 inhibitor enhances mitochondrial quality and cell viability by regulating NMNAT3-PARP1 axis. Abbreviations: LPS, lipopolysaccharide; NMN, nicotinamide mononucleotide; NMNAT1, Nicotinamide mononucleotide adenylyl transferase 1; NMNAT3, Nicotinamide mononucleotide adenylyl transferase 3; NAD^+, Nicotinamide adenine dinucleotide; PARP1, Poly (ADP-ribose) polymerase-1; PAR, poly ADP-ribose. Created with BioRender.com

of PARP1, and improved mitophagy. However, NMN supplementation also led to higher PARylation modification levels and sustained MMP damage. The change in MMP may be attributed to higher PARylation levels caused by NMN supplementation, which consistent with previous studies [27, 62]. Mechanistic studies have demonstrated that upregulated PARylation mediates MMP collapse via the parthanatos pathway [63], which is a form of cell death triggered by the hyperactivation of PARP1. The hyperactivated PARP1 stimulates PARylation and the translocation of AIFs to the nucleus, thereby accelerating the depletion of NAD^+ and ATP. This type of cell death is characterized by key features such as PARP1-dependence and energetic collapse [64].

PARP1 acts as a sensor, transducer, and effector of DNA damage [65], and plays a major role in cell death relevant to neurologic disorders [66, 67]. The main product catalyzed by PARP1 are PAR polymer, which reflect its activity [68]. Kam et al. have shown that PAR polymer accelerates the formation of pathological α-syn, leading to neurotoxicity [66]. In this study, we observed a significant increase in PARylation modification levels and PARP1 expression in neuroinflammatory mice and cell models. Our findings align with a previous observation of PARP1 activation in a neuroinflammatory cell models [69], making PARP1 a possible target for anti-inflammatory treatment of microglia. Therapeutic effects on various neurodegenerative diseases can be achieved through PARP1 inhibition and *PARP1* gene knockout [66, 67, 70]. Notably, NMNAT3 knockout exhibited higher PARylation modification levels, suggesting that the PARylation is regulated by NMNAT3.

In order to further examine the impact of PAPR1, we utilized a PAPR1 inhibitor, PJ-34. The results showed that the combination of NMN and PJ-34 promoted cell viability and mitochondrial quality more effectively than NMN alone. Specifically, our results revealed that NMN and PJ-34 could reduce mitochondrial fission, increase mitochondrial fusion, normalize mitochondrial morphology, and increase MMP and ATP levels. Moreover, the level of mitophagy was further increased under NMN and PJ-34 administration.

To assess mitochondrial function, several parameters were examined, including mitochondrial morphology,

ATP content, and MMP. As anticipated, LPS administration resulted in reduced mitochondrial volume, as well as significant decreases in ATP content and MMP. These findings suggest excessive mitochondrial division and impaired mitochondrial function. Normally, damaged mitochondria are eliminated through mitophagy [71]. However, further investigations demonstrated a decrease in the co-localization of the lysosomal marker LAMP1 and mitochondria following LPS treatment, indicating incomplete mitophagy.

FoxO1 is a key transcription factor downstream of PARP1, which binds to target genes to mediate gene transcription regulation. Recent studies have reported that FoxO1 plays a crucial role in maintaining mitochondrial homeostasis by binding to the *PINK1* promoter and influencing PINK1/Parkin-mediated mitophagy [72, 73]. It is suggested that FoxO1 may be a transcription factor regulating PINK1, which is sufficient for Parkin recruitment and mitophagy [74]. In this study, we observed that the binding of FoxO1 to the *PINK1* promoter and the levels of *PINK1* mRNA decreased under the action of LPS, and increased when NMN and PJ-34 were added. This confirmed that PARP1 activates PINK1/Parkin-mediated mitophagy by promoting the binding of FoxO1 to the *PINK1* promoter.

Among the intriguing questions raised by these data is how NMNAT3 affects PARylation. NMNAT3 is a specific enzyme for mitochondrial NAD^+ synthesis [75], while PARP1 is the main NAD^+ -consuming enzyme in nucleus [76]. NAD^+ is spatially inherent in distinct subcellular compartments owing to its segregated NAD^+ synthase and consuming enzymes [17]. However, studies have shown that NAD^+ has a crosstalk between nucleus and mitochondria [77, 78]. The reduction of mitochondrial NAD^+ may promote the distribution and availability of nuclear NAD^+, thereby facilitating the process of ADP-ribosylation in the nucleus. Overall, while our study confirms the crucial role of NMNAT3 in PARylation, the detailed mechanisms of the crosstalk between mitochondrial and nuclear NAD^+ remain to be further elucidated.

Conclusion

In summary, our study demonstrates that in LPS-induced neuroinflammation, the mitochondrial-specific NAD^+ synthase NMNAT3 was significantly down-regulated, leading to the upregulation of nuclear NAD^+ consuming enzyme PARP1, revealing a novel pathological mechanism of neuroinflammation. On one hand, the downregulation of NMNAT3 may precede the production of inflammatory factors, resulting in accumulation of PAR polymer, downregulation of autophagy initiation process, and the damage of mitochondria. On the other hand, the activation of PARP1 further impairs mitophagy, mitochondrial ultrastructure, mitochondrial dynamics and mitochondrial function. Moreover, PARP1 activation inhibits PINK1/Parkin-mediated mitophagy by disrupting the binding of FoxO1 to the *PINK1* promoter. These effects can be reversed by supplementing with NMN and PARP1 inhibitor PJ-34. This pathogenic mechanism underscores the critical role of NMNAT3-PARP1 axis in neuroinflammation, and provides valuable insights into the development of therapeutic strategies for neuroinflammation and neurodegenerative diseases.

Abbreviations

PARP1	Poly (ADP-ribose) polymerase-1
NMNAT3	Nicotinamide mononucleotide adenylyl transferase 3
NAD^+	Nicotinamide adenine dinucleotide
CD38/CD157	Cyclic ADP-ribose synthases
SARM1	Sterile Alpha and Toll/Interleukin-1 Receptor Motif-Containing 1
NA	Nicotinic acid
NAM	Nicotinamide
NMN	Nicotinamide mononucleotide
PAR	Poly ADP-ribose
ICV	Intracerebroventricular
MMP	Mitochondrial membrane potential
AIFs	Apoptosis-inducing factors
LAMP1	Lysosomal-associated membrane protein 1
PINK1	PTEN induced kinase 1
FoxO1	Forkhead box O1

Supplementary Information

The online version contains supplementary material available at https://doi.org/10.1186/s12967-025-06280-1.

Supplementary Material 1

Author contributions

Study concept and design: JL, XC, YY, JL*; drafting of the manuscript: JL, XC, YY, JL*; acquisition, analysis, or interpretation of data: JL, RM, BZ; critical revision of the manuscript for important intellectual content: JL, YZ, MW. All authors have read and approved the final manuscript.

Funding

This work was supported by National Natural Science Foundation of China (82160759, 82060792, 82101333), Natural Science Foundation of Ningxia (2024AAC02049, 2024AAC03294), and Key R&D Program of Ningxia (2021BEG03100).

Data availability

Data will be made available on reasonable request.

Declarations

Ethics approval and consent to participate

The animal protocol was approved by the Institutional Animal Care and Use Committee (IACUC–NYLAC-2022-N180).

Consent for publication

Not applicable.

Competing interests

The authors declare that they have no known competing financial interests or personal relationships that could have appeared to influence the work reported in this paper.

Received: 30 October 2024 / Accepted: 20 February 2025
Published online: 06 March 2025

References

1. Han B, Jiang W, Cui P, Zheng K, Dang C, Wang J, Li H, Chen L, Zhang R, Wang QM, Ju Z. Hao. Microglial PGC-1alpha protects against ischemic brain injury by suppressing neuroinflammation. Genome Med. 2021;13(1):47. https://doi.org/10.1186/s13073-021-00863-5.
2. Nakano-Kobayashi A, Fukumoto A, Morizane A, Nguyen DT, Le TM, Hashida K, Hosoya T, Takahashi R, Takahashi J, Hori O. Hagiwara. Therapeutics potentiating microglial p21-Nrf2 axis can rescue neurodegeneration caused by neuroinflammation. Sci Adv. 2020;6(46). https://doi.org/10.1126/sciadv.abc1428.
3. Li R, Li X, Zhao J, Meng F, Yao C, Bao E, Sun N, Chen X, Cheng W, Hua H, Li X, Wang B, Wang H, Pan X, You H, Yang J, Ikezoe T. Mitochondrial STAT3 exacerbates LPS-induced sepsis by driving CPT1a-mediated fatty acid oxidation. Theranostics. 2022;12(2):976–98. https://doi.org/10.7150/thno.63751.
4. Ahuja M, Ammal Kaidery N, Attucks OC, McDade E, Hushpulian DM, Gaisin A, Gaisina I, Ahn YH, Nikulin S, Poloznikov A, Gazaryan I, Yamamoto M, Matsumoto M, Igarashi K, Sharma SM. Thomas. Bach1 derepression is neuroprotective in a mouse model of Parkinson's disease. Proc Natl Acad Sci U S A. 2021;118(45). https://doi.org/10.1073/pnas.2111643118.
5. Zhang Q, Song Q, Yu R, Wang A, Jiang G, Huang Y, Chen J, Xu J, Wang D, Chen H. Gao. Nano-Brake halts mitochondrial dysfunction cascade to alleviate neuropathology and rescue Alzheimer's cognitive deficits. Adv Sci (Weinh). 2023;10(7):e2204596. https://doi.org/10.1002/advs.202204596.
6. Navarro MN, Gomez de Las Heras MM, Mittelbrunn M. Nicotinamide adenine dinucleotide metabolism in the immune response, autoimmunity and inflammageing. Br J Pharmacol. 2022;179(9):1839–56. https://doi.org/10.1111/bph.15477.
7. Byun J, Oka SI, Imai N, Huang CY, Ralda G, Zhai P, Ikeda Y, Ikeda S, Sadoshima J. Both gain and loss of Nampt function promote pressure overload-induced heart failure. Am J Physiol Heart Circ Physiol. 2019;317(4):H711–25. https://doi.org/10.1152/ajpheart.00222.2019.
8. Huang G, He Y, Hong L, Zhou M, Zuo X, Zhao Z. Restoration of NAD^+ homeostasis protects C2C12 myoblasts and mouse levator Ani muscle from mechanical stress-induced damage. Anim Cells Syst (Seoul). 2022;26(4):192–202. https://doi.org/10.1080/19768354.2022.2106303
9. Li HR, Liu Q, Zhu CL, Sun XY, Sun CY, Yu CM, Li P, Deng XM. Wang. beta-Nicotinamide mononucleotide activates NAD^+/SIRT1 pathway and attenuates inflammatory and oxidative responses in the hippocampus regions of septic mice. Redox Biol. 2023;63102745. https://doi.org/10.1016/j.redox.2023.102745
10. Sano H, Kratz A, Nishino T, Imamura H, Yoshida Y, Shimizu N, Kitano H. Yachie. Nicotinamide mononucleotide (NMN) alleviates the poly(I:C)-induced inflammatory response in human primary cell cultures. Sci Rep. 2023;13(1):11765. https://doi.org/10.1038/s41598-023-38762-x.
11. Wang T, Zhang F, Peng W, Wang L, Zhang J, Dong W, Tian X, Ye C, Li Y, Gong Y. Overexpression of NMNAT3 improves mitochondrial function and enhances antioxidative stress capacity of bone marrow mesenchymal stem cells via the NAD^+-Sirt3 pathway. Biosci Rep. 2022;42(1). https://doi.org/10.1042/BSR20211005
12. Gulshan M, Yaku K, Okabe K, Mahmood A, Sasaki T, Yamamoto M, Hikosaka K, Usui I, Kitamura T, Tobe K. Nakagawa. Overexpression of Nmnat3 efficiently increases NAD and NGD levels and ameliorates age-associated insulin resistance. Aging Cell. 2018;17(4):e12798. https://doi.org/10.1111/acel.12798.
13. Gu Y, Gao L, He J, Luo M, Hu M, Lin Y, Li J, Hou T, Si J. Yu. beta-Nicotinamide mononucleotide supplementation prolongs the lifespan of prematurely aged mice and protects colon function in ageing mice. Food Funct. 2024;15(6):3199–213. https://doi.org/10.1039/d3fo05221d.
14. Quesada A, O'Valle F, Montoro-Molina S, Gomez-Morales M, Caba-Molina M, Gonzalez JF, de Gracia MC, Osuna A, Vargas F. Wangensteen. 5-aminoisoquinoline improves renal function and fibrosis during recovery phase of cisplatin-induced acute kidney injury in rats. Biosci Rep. 2018;38(2). https://doi.org/10.1042/BSR20171313.
15. Scheibye-Knudsen M, Mitchell SJ, Fang EF, Iyama T, Ward T, Wang J, et al. A high-fat diet and NAD^+ activate Sirt1 to rescue premature aging in Cockayne syndrome. Cell Metab. 2014;20(5):840–55. https://doi.org/10.1016/j.cmet.2014.10.005
16. Samer S, Arif MS, Giron LB, Zukurov JPL, Hunter J, Santillo BT, et al. Nicotinamide activates latent HIV-1 ex vivo in ART suppressed individuals, revealing higher potency than the association of two methyltransferase inhibitors, Chaetocin and BIX01294. Braz J Infect Dis. 2020;24(2):150–59. https://doi.org/10.1016/j.bjid.2020.01.005.
17. Ryu KW, Nandu T, Kim J, Challa S, DeBerardinis RJ. Kraus. Metabolic regulation of transcription through compartmentalized NAD^+ biosynthesis. Science. 2018;360(6389). https://doi.org/10.1126/science.aan5780
18. Li C, Wu J, Dong Q, Ma J, Liu G, Gao H, et al. The crosstalk between oxidative stress and DNA damage induces neural stem cell senescence by HO-1/PARP1 non-canonical pathway. Free Radic Biol Med. 2024. https://doi.org/10.1016/j.freeradbiomed.2024.07.020.
19. Yang X, Li G, Lou P, Zhang M, Yao K, Xiao J, Chen Y, Xu J, Tian S, Deng M, Pan Y, Li M, Wu X, Liu R, Shi X, Tian Y, Yu L, Ke H, Jiao B, Cong Y, Plikus MV, Liu X, Yu Z, Lv C. Excessive nucleic acid R-loops induce mitochondria-dependent epithelial cell necroptosis and drive spontaneous intestinal inflammation. Proc Natl Acad Sci U S A. 2024;121(1):e2307395120. https://doi.org/10.1073/pnas.2307395120.
20. Kovacs D, Vantus VB, Vamos E, Kalman N, Schicho R, Gallyas F, et al. Olaparib: a clinically applied PARP inhibitor protects from experimental Crohn's disease and maintains barrier integrity by improving bioenergetics through rescuing glycolysis in colonic epithelial cells. Oxid Med Cell Longev. 2021;20217308897. https://doi.org/10.1155/2021/7308897
21. Fang EF, Scheibye-Knudsen M, Brace LE, Kassahun H, SenGupta T, Nilsen H, et al. Defective mitophagy in XPA via PARP-1 hyperactivation and NAD^+/SIRT1 reduction. Cell. 2014;157(4):882–96. https://doi.org/10.1016/j.cell.2014.03.026
22. Bai P. Biology of Poly(ADP-Ribose) polymerases: the factotums of cell maintenance. Mol Cell. 2015;58(6):947–58. https://doi.org/10.1016/j.molcel.2015.01.034.
23. Curtin NJ, Szabo C. Poly(ADP-ribose) polymerase Inhibition: past, present and future. Nat Rev Drug Discov. 2020;19(10):711–36. https://doi.org/10.1038/s41573-020-0076-6.
24. Klimova N, Kristian T. Multi-targeted effect of nicotinamide mononucleotide on brain bioenergetic metabolism. Neurochem Res. 2019;44(10):2280–87. https://doi.org/10.1007/s11064-019-02729-0.
25. Crisol BM, Veiga CB, Braga RR, Lenhare L, Baptista IL, Gaspar RC, et al. NAD^+ precursor increases aerobic performance in mice. Eur J Nutr. 2020;59(6):2427–37. https://doi.org/10.1007/s00394-019-02089-z
26. Zhang Q, Li Z, Li Q, Trammell SA, Schmidt MS, Pires KM, et al. Control of NAD^+ homeostasis by autophagic flux modulates mitochondrial and cardiac function. EMBO J. 2024;43(3):362–90. https://doi.org/10.1038/s44318-023-00009-w
27. Baek SH, Bae ON, Kim EK, Yu SW. Induction of mitochondrial dysfunction by poly(ADP-ribose) polymer: implication for neuronal cell death. Mol Cells. 2013;36(3):258–66. https://doi.org/10.1007/s10059-013-0172-0.
28. El-Sahar AE, Shiha NA, El Sayed NS. Ahmed. Alogliptin attenuates Lipopolysaccharide-Induced neuroinflammation in mice through modulation of TLR4/MYD88/NF-kappaB and miRNA-155/SOCS-1 signaling pathways. Int J Neuropsychopharmacol. 2021;24(2):158–69. https://doi.org/10.1093/ijnp/pyaa078.
29. Lawson MA, Parrott JM, McCusker RH, Dantzer R, Kelley KW. O'Connor. Intracerebroventricular administration of lipopolysaccharide induces indoleamine-2,3-dioxygenase-dependent depression-like behaviors. J Neuroinflammation. 2013;1087. https://doi.org/10.1186/1742-2094-10-87.
30. Xu H, Lotfy P, Gelb S, Pragana A, Hehnly C, Byer LIJ, Shipley FB, Zawadzki ME, Cui J, Deng L, Taylor M, Webb M, Lidov HGW, Andermann ML, Chiu IM, Ordovas-Montanes J. Lehtinen. The choroid plexus synergizes with immune cells during neuroinflammation. Cell. 2024;187(18):4946–e6317. https://doi.org/10.1016/j.cell.2024.07.002.
31. Nam HY, Nam JH, Yoon G, Lee JY, Nam Y, Kang HJ, Cho HJ, Kim J. Hoe. Ibrutinib suppresses LPS-induced neuroinflammatory responses in BV2 microglial cells and wild-type mice. J Neuroinflammation. 2018;15(1):271. https://doi.org/10.1186/s12974-018-1308-0.
32. Li JM, Hu T, Zhou XN, Zhang T, Guo JH, Wang MY, Wu YL, Su WJ. Jiang. The involvement of NLRP3 inflammasome in CUMS-induced AD-like pathological changes and related cognitive decline in mice. J Neuroinflammation. 2023;20(1):112. https://doi.org/10.1186/s12974-023-02791-0.
33. Sambamoorthy G, Raman K. Understanding the evolution of functional redundancy in metabolic networks. Bioinformatics. 2018;34(17):i981–87. https://doi.org/10.1093/bioinformatics/bty604.
34. Cheng XT, Xie YX, Zhou B, Huang N, Farfel-Becker T. Sheng. Characterization of LAMP1-labeled nondegradative lysosomal and endocytic compartments in neurons. J Cell Biol. 2018;217(9):3127–39. https://doi.org/10.1083/jcb.201711083.
35. Chen C, Yang C, Wang J, Huang X, Yu H, Li S, Li S, Zhang Z, Liu J, Yang X, Liu GP. Melatonin ameliorates cognitive deficits through improving mitophagy in a

mouse model of Alzheimer's disease. J Pineal Res. 2021;71(4):e12774. https://doi.org/10.1111/jpi.12774.
36. Shi Q, Cheng Q, Chen C. The role of autophagy in the pathogenesis of ischemic stroke. Curr Neuropharmacol. 2021;19(5):629–40. https://doi.org/10.2174/1570159X18666200729101913.
37. Zhong Q, Zheng K, Li W, An K, Liu Y, Xiao X, Hai S, Dong B, Li S, An Z, Dai L. Post-translational regulation of muscle growth, muscle aging and sarcopenia. J Cachexia Sarcopenia Muscle. 2023;14(3):1212–27. https://doi.org/10.1002/jcsm.13241.
38. Prerna K, Dubey VK. Beclin1-mediated interplay between autophagy and apoptosis: new Understanding. Int J Biol Macromol. 2022. https://doi.org/10.1016/j.ijbiomac.2022.02.005. 204258-73.
39. Sowers ML. Sowers. Glioblastoma and methionine addiction. Int J Mol Sci. 2022;23(13). https://doi.org/10.3390/ijms23137156.
40. Okur MN, Fang EF, Fivenson EM, Tiwari V, Croteau DL, Bohr VA. Cockayne syndrome proteins CSA and CSB maintain mitochondrial homeostasis through NAD^+ signaling. Aging Cell. 2020;19(12):e13268. https://doi.org/10.1111/acel.13268
41. Schondorf DC, Ivanyuk D, Baden P, Sanchez-Martinez A, De Cicco S, Yu C, Giunta I, Schwarz LK, Di Napoli G, Panagiotakopoulou V, Nestel S, Keatinge M, Pruszak J, Bandmann O, Heimrich B, Gasser T, Whitworth AJ. Deleidi. The NAD + Precursor nicotinamide riboside rescues mitochondrial defects and neuronal loss in iPSC and fly models of Parkinson's disease. Cell Rep. 2018;23(10):2976–88. https://doi.org/10.1016/j.celrep.2018.05.009.
42. Jang KH, Hwang Y, Kim E. PARP1 impedes SIRT1-Mediated autophagy during degeneration of the retinal pigment epithelium under oxidative stress. Mol Cells. 2020;43(7):632–44. https://doi.org/10.14348/molcells.2020.0078.
43. Mao K, Zhang G. The role of PARP1 in neurodegenerative diseases and aging. FEBS J. 2022;289(8):2013–24. https://doi.org/10.1111/febs.15716.
44. Larson-Casey JL, Deshane JS, Ryan AJ, Thannickal VJ, Carter AB. Macrophage Akt1 Kinase-Mediated mitophagy modulates apoptosis resistance and pulmonary fibrosis. Immunity. 2016;44(3):582–96. https://doi.org/10.1016/j.immuni.2016.01.001.
45. Hou S, Song Y, Sun D, Zhu S, Wang Z. Xanthohumol-Induced rat glioma C6 cells death by triggering mitochondrial stress. Int J Mol Sci. 2021;22(9). https://doi.org/10.3390/ijms22094506.
46. Scheibye-Knudsen M, Fang EF, Croteau DL, Bohr VA. Contribution of defective mitophagy to the neurodegeneration in DNA repair-deficient disorders. Autophagy. 2014;10(8):1468–9. https://doi.org/10.4161/auto.29321.
47. Yamano K, Sawada M, Kikuchi R, Nagataki K, Kojima W, Endo R, Kinefuchi H, Sugihara A, Fujino T, Watanabe A, Tanaka K, Hayashi G, Murakami H. Matsuda. Optineurin provides a mitophagy contact site for TBK1 activation. EMBO J. 2024;43(5):754–79. https://doi.org/10.1038/s44318-024-00036-1.
48. Tsukamoto H, Takeuchi S, Kubota K, Kobayashi Y, Kozakai S, Ukai I, Shichiku A, Okubo M, Numasaki M, Kanemitsu Y, Matsumoto Y, Nochi T, Watanabe K, Aso H. Tomioka. Lipopolysaccharide (LPS)-binding protein stimulates CD14-dependent Toll-like receptor 4 internalization and LPS-induced TBK1-IKKε-IRF3 axis activation. J Biol Chem. 2018;293(26):10186–201. https://doi.org/10.1074/jbc.M117.796631.
49. Wang J, Wang J, Hong W, Zhang L, Song L, Shi Q, Shao Y, Hao G, Fang C, Qiu Y, Yang L, Yang Z, Wang J, Cao J, Yang B, He Q. Weng. Optineurin modulates the maturation of dendritic cells to regulate autoimmunity through JAK2-STAT3 signaling. Nat Commun. 2021;12(1):6198. https://doi.org/10.1038/s41467-021-26477-4.
50. Liu L, Li J, Ke Y, Zeng X, Gao J, Ba X, Wang R. The key players of Parthanatos: opportunities for targeting multiple levels in the therapy of parthanatos-based pathogenesis. Cell Mol Life Sci. 2022;79(1):60. https://doi.org/10.1007/s00018-021-04109-w.
51. Huang P, Chen G, Jin W, Mao K, Wan H, He Y. Molecular mechanisms of parthanatos and its role in diverse diseases. Int J Mol Sci. 2022;23(13):7292. https://doi.org/10.3390/ijms23137292.
52. Virag L, Scott GS, Cuzzocrea S, Marmer D, Salzman AL, Szabo C. Peroxynitrite-induced thymocyte apoptosis: the role of caspases and Poly (ADP-ribose) synthetase (PARS) activation. Immunology. 1998;94(3):345–55. https://doi.org/10.1046/j.1365-2567.1998.00534.x.
53. Pokharel MD, Garcia-Flores A, Marciano D, Franco MC, Fineman JR, Aggarwal S, Wang T. Black. Mitochondrial network dynamics in pulmonary disease: bridging the gap between inflammation, oxidative stress, and bioenergetics. Redox Biol. 2024;70103049. https://doi.org/10.1016/j.redox.2024.103049.
54. Zhao Q, Lu D, Wang J, Liu B, Cheng H, Mattson MP, Cheng A. Calcium dysregulation mediates mitochondrial and neurite outgrowth abnormalities in SOD2 deficient embryonic cerebral cortical neurons. Cell Death Differ. 2019;26(9):1600–14. https://doi.org/10.1038/s41418-018-0230-4.
55. Kinoshita A, Locher L, Tienken R, Meyer U, Danicke S, Rehage J, Huber K. Associations between forkhead box O1 (FoxO1) expression and indicators of hepatic glucose production in transition dairy cows supplemented with dietary nicotinic acid. PLoS ONE. 2016;11(1):e0146670. https://doi.org/10.1371/journal.pone.0146670.
56. Czapski GA, Cieslik M, Wencel PL, Wojtowicz S, Strosznajder RP, Strosznajder JB. Inhibition of poly(ADP-ribose) polymerase-1 alters expression of mitochondria-related genes in PC12 cells: relevance to mitochondrial homeostasis in neurodegenerative disorders. Biochim Biophys Acta Mol Cell Res. 2018;1865(2):281–88. https://doi.org/10.1016/j.bbamcr.2017.11.003.
57. Li W, Du M, Wang Q, Ma X, Wu L, Guo F, Ji H, Huang F, Qin G. FoxO1 promotes mitophagy in the podocytes of diabetic male mice via the PINK1/Parkin pathway. Endocrinology. 2017;158(7):2155–67. https://doi.org/10.1210/en.2016-1970.
58. Fortunato C, Mazzola F, Raffaelli N. The key role of the NAD biosynthetic enzyme nicotinamide mononucleotide adenylyltransferase in regulating cell functions. IUBMB Life. 2022;74(7):562–72. https://doi.org/10.1002/iub.2584.
59. McReynolds MR, Chellappa K, Chiles E, Jankowski C, Shen Y, Chen L, et al. NAD^+ flux is maintained in aged mice despite lower tissue concentrations. Cell Syst. 2021;12(12):1160–e724. https://doi.org/10.1016/j.cels.2021.09.001
60. Hussein MM, Sayed RKA, Mokhtar DM. Structural and immunohistochemical analysis of the cellular compositions of the liver of Molly fish (Poecilia sphenops), focusing on its immune role. Zoological Lett. 2023;9(1):1. https://doi.org/10.1186/s40851-022-00200-7.
61. Cheng F, Zhang Y, Xiong H, Zhao M, Wang Q, Zhu Y, et al. NMNATs expression Inhibition mediated NAD^+ deficiency plays a critical role in doxorubicin-induced hepatotoxicity in mice. Toxicol Appl Pharmacol. 2024;482116799. https://doi.org/10.1016/j.taap.2023.116799
62. Jiang HY, Yang Y, Zhang YY, Xie Z, Zhao XY, Sun Y. Kong. The dual role of poly(ADP-ribose) polymerase-1 in modulating parthanatos and autophagy under oxidative stress in rat cochlear marginal cells of the stria vascularis. Redox Biol. 2018;14361–70. https://doi.org/10.1016/j.redox.2017.10.002.
63. Wan H, Chen H, Liu J, Yang B, Zhang Y, Bai Y, et al. PARP1 Inhibition prevents oxidative stress in age-related hearing loss via PAR-Ca^{2+}-AIF axis in cochlear strial marginal cells. Free Radic Biol Med. 2024;220222–35. https://doi.org/10.1016/j.freeradbiomed.2024.05.020
64. Robinson N, Ganesan R, Hegedus C, Kovacs K, Kufer TA, Virag L. Programmed necrotic cell death of macrophages: focus on pyroptosis, necroptosis, and parthanatos. Redox Biol. 2019;26101239. https://doi.org/10.1016/j.redox.2019.101239.
65. Fischbach A, Kruger A, Hampp S, Assmann G, Rank L, Hufnagel M, Stockl MT, Fischer JMF, Veith S, Rossatti P, Ganz M, Ferrando-May E, Hartwig A, Hauser K, Wiesmuller L, Burkle A, Mangerich A. The C-terminal domain of p53 orchestrates the interplay between non-covalent and covalent poly(ADP-ribosyl)ation of p53 by PARP1. Nucleic Acids Res. 2018;46(2):804–22. https://doi.org/10.1093/nar/gkx1205.
66. Kam TI, Mao X, Park H, Chou SC, Karuppagounder SS, Umanah GE, Yun SP, Brahmachari S, Panicker N, Chen R, Andrabi SA, Qi C, Poirier GG, Pletnikova O, Troncoso JC, Bekris LM, Leverenz JB, Pantelyat A, Ko HS, Rosenthal LS, Dawson TM. Dawson. Poly(ADP-ribose) drives pathologic alpha-synuclein neurodegeneration in Parkinson's disease. Science. 2018;362(6414). https://doi.org/10.1126/science.aat8407.
67. Ma QW, Han RT, Wu ZJ, Zhou JJ, Chen MT, Zhang XZ. Ma, N. Feng. Melatonin derivative 6a as a PARP-1 inhibitor for the treatment of Parkinson's disease. Front Pharmacol. 2024;151363212. https://doi.org/10.3389/fphar.2024.1363212.
68. Zhao S, Hong Y, Liang YY, Li XL, Shen JC, Sun CC, et al. Compartmentalized regulation of NAD^+ by Di (2-ethyl-hexyl) phthalate induces DNA damage in placental trophoblast. Redox Biol. 2022;55102414. https://doi.org/10.1016/j.redox.2022.102414
69. Diestel A, Aktas O, Hackel D, Hake I, Meier S, Raine CS, Nitsch R, Zipp F, Ullrich O. Activation of microglial poly(ADP-ribose)-polymerase-1 by cholesterol breakdown products during neuroinflammation: a link between demyelination and neuronal damage. J Exp Med. 2003;198(11):1729–40. https://doi.org/10.1084/jem.20030975.
70. Wang Y, Pleasure D, Deng W, Guo F. Therapeutic potentials of Poly (ADP-Ribose) polymerase 1 (PARP1) Inhibition in multiple sclerosis and animal models: concept revisiting. Adv Sci (Weinh). 2022;9(5):e2102853. https://doi.org/10.1002/advs.202102853.

71. Li HM, Liu X, Meng ZY, Wang L, Zhao LM, Chen H, Wang ZX, Cui H, Tang XQ, Li XH, Han WN, Bai X, Lin Y, Liu H, Zhang Y. Yang. Kanglexin delays heart aging by promoting mitophagy. Acta Pharmacol Sin. 2022;43(3):613–23. https://doi.org/10.1038/s41401-021-00686-5.
72. Wang D, Wang Y, Zou X, Shi Y, Liu Q, Huyan T, Su J, Wang Q, Zhang F, Li X, Tie L. FOXO1 Inhibition prevents renal ischemia-reperfusion injury via cAMP-response element binding protein/PPAR-gamma coactivator-1alpha-mediated mitochondrial biogenesis. Br J Pharmacol. 2020;177(2):432–48. https://doi.org/10.1111/bph.14878.
73. Zhao N, Xia J, Xu B. Physical exercise May exert its therapeutic influence on Alzheimer's disease through the reversal of mitochondrial dysfunction via SIRT1-FOXO1/3-PINK1-Parkin-mediated mitophagy. J Sport Health Sci. 2021;10(1):1–3. https://doi.org/10.1016/j.jshs.2020.08.009.
74. Narendra DP, Jin SM, Tanaka A, Suen DF, Gautier CA, Shen J, Cookson MR. Youle. PINK1 is selectively stabilized on impaired mitochondria to activate parkin. PLoS Biol. 2010;8(1):e1000298. https://doi.org/10.1371/journal.pbio.1000298.
75. Yoshino J, Baur JA, Imai SI. NAD^+ intermediates: the biology and therapeutic potential of NMN and NR. Cell Metab. 2018;27(3):513–28. https://doi.org/10.1016/j.cmet.2017.11.002
76. Lee S, Kim J, Chung WC, Han JH, Song MJ. Epstein-Barr virus viral processivity factor EA-D facilitates virus lytic replication by inducing Poly(ADP-Ribose) polymerase 1 degradation. J Virol. 2022;96(21):e0037122. https://doi.org/10.1128/jvi.00371-22.
77. Guldenpfennig A, Hopp AK, Muskalla L, Manetsch P, Raith F, Hellweg L, et al. Absence of mitochondrial SLC25A51 enhances PARP1-dependent DNA repair by increasing nuclear NAD^+ levels. Nucleic Acids Res. 2023;51(17):9248–65. https://doi.org/10.1093/nar/gkad659
78. Hopp AK, Teloni F, Bisceglie L, Gondrand C, Raith F, Nowak K, et al. Mitochondrial NAD^+ Controls Nuclear ARTD1-Induced ADP-Ribosylation. Mol Cell. 2021;81(2):340– 54 e5. https://doi.org/10.1016/j.molcel.2020.12.034

Publisher's note